

## Derivation and Characterization of Ubiquitin-Specific Protease 18 Inhibitors

Blessing Ogunlade<sup>1</sup>, Kevin Dalby<sup>2,3</sup>, Samuel C. Okpechi<sup>1</sup>, Eun Jeong Cho<sup>2,3</sup>, Liliya Tyutyunyk-Massey<sup>1</sup>, Zibo Chen<sup>1</sup>, Xiuxia Liu<sup>1</sup>, Joseph Ivanic<sup>4</sup>, Brian Luke<sup>4</sup>, Shyamal D. Desai<sup>5</sup>, Yair Alfaro<sup>1</sup>, Ashwini K. Devkota<sup>2,3</sup>, Rae M. Sammons<sup>2,3</sup>, Gilbert G. Privé<sup>6,7,8</sup>, Xi Liu<sup>1</sup>,  
and Ethan Dmitrovsky<sup>1\*</sup>

From the <sup>1</sup>Molecular Pharmacology Program, Cancer Research Technology Program, Frederick National Laboratory for Cancer Research, Frederick, MD 21702-1201; <sup>2</sup>Targeted Therapeutic Drug Discovery and Development Program, <sup>3</sup>Division of Chemical Biology and Medicinal Chemistry, The University of Texas at Austin, Austin, Texas; <sup>4</sup>Advanced Biomedical Computational Science, Frederick National Laboratory for Cancer Research, Frederick, MD 21702-1201; <sup>5</sup>Department of Biochemistry and Molecular Biology, Louisiana State University Health Science Center-School of Medicine, New Orleans, LA; <sup>6</sup>Division of Cancer Genomics and Proteomics, Ontario Cancer Institute, <sup>7</sup>Department of Medical Biophysics and <sup>8</sup>Department of Biochemistry, University of Toronto, Toronto, Ontario, Canada.

\*Address correspondence to:

Ethan Dmitrovsky, MD

Frederick National Laboratory for Cancer Research

PO Box B, Frederick, MD 21701

Phone: 301-846-1154 Email: [ethan.dmitrovsky@gmail.com](mailto:ethan.dmitrovsky@gmail.com)

Keywords:  $\beta$ -lapachone, USP18 inhibitors and lung cancer

Conflicts of Interest: No conflicts of interest are cited by these authors.

## Abstract

Ubiquitin-Specific Protease 18 (USP18) is a deISGylation enzyme and antineoplastic target. To develop USP18 inhibitors, an enzymatically active human recombinant USP18 protein was engineered suitable for high-throughput screening of ~80,000 chemical compounds. Three of them substantially inhibited USP18 enzymatic activity with  $\beta$ -lapachone having prominent antineoplastic activity. Independent  $\beta$ -lapachone treatments of murine and human lung cancer cell lines statistically-significantly reduced proliferation and increased apoptosis. Gain of USP18 expression antagonized these effects.  $\beta$ -lapachone treatments statistically-significantly repressed lung cancer xenograft growth.  $\beta$ -lapachone increased reactive oxygen species (ROS), but antineoplastic effects occurred at dosages with negligible ROS production. ROS scavenger treatments did not rescue  $\beta$ -lapachone effects at these concentrations, consistent with an ROS-independent mechanism. Interferon-Stimulated Response Element (ISRE) reporter assays following  $\beta$ -lapachone treatment activated this reporter. USP18 co-transfection antagonized this activity.  $\beta$ -lapachone treatments increased global ISGylation. RNA sequencing of lung cancer cells engineered with or without enhanced USP18 expression showed specific pathways affected by  $\beta$ -lapachone treatment. Proteomic analysis of these treated cells revealed known and new ISGylated proteins. *In silico* modeling identified a unique USP18 pocket where these USP18 inhibitors bind. Engineered mutation of this pocket disrupted  $\beta$ -lapachone activity. Taken together,  $\beta$ -lapachone is an antineoplastic tool compound useful for USP18 inhibitor development.

## Introduction

Lung cancer is the leading cause of cancer-related deaths (1). Despite advances in surgery, radiation, chemotherapy, targeted therapy, and immunotherapy, five-year survival for all lung cancer stages is only 28% (1). Most lung cancer patients are diagnosed at stage IV where the five-year survival rate is far less than for all other stages (1, 2). While targeted treatments such as with EGFR, BRAF, and ALK inhibitors improved outcomes in subsets of lung cancer patients, these therapies are active in only a minority of lung cancer patients. Adding to the need for new antineoplastics in lung cancer is the frequent onset of resistance to current anti-cancer agents. These challenges indicate the need for novel strategies to improve lung cancer survival, as explored here.

Ubiquitination, a post-translational modification, regulates diverse cellular processes, including protein stability, signal transduction, immune response, and other processes (3, 4). A related system involves ISGylation, an interferon-regulated pathway that modifies target proteins in a manner analogous to that of ubiquitination (5, 6). This pathway involves a set of enzymes that include E1-like activating enzyme (UBE1L) (7-9), E2-conjugating enzyme (UBCH8) (10, 11), and E3 ligase (HERC5A and others) (12, 13). Together, this pathway facilitates Interferon-Stimulated Gene 15 (ISG15) conjugation to substrate proteins (14-16).

Ubiquitin-specific protease 18 (USP18) is the enzyme that deconjugates ISG15 from its substrates, reversing ISGylation (17, 18). Beyond its canonical role in interferon

signaling, USP18 is implicated in tumorigenesis, where it stabilizes oncogenic proteins like PML/RAR $\alpha$ , cyclin D1, and KRAS that in turn promote carcinogenesis (19-29). Thus, pharmacologic USP18 inhibitors are hypothesized to address a previously unmet need in oncology.

To address this knowledge gap, we developed an enzymatically active recombinant USP18 protein and performed a high-throughput screen to identify small-molecule inhibitors of the USP18 enzymatic activity. This and subsequent screens reported here identified  $\beta$ -lapachone as an USP18 inhibitor with anti-cancer activity.

$\beta$ -lapachone is a naturally occurring quinone product derived from the bark of *Tabebuia avellanedae*, with anti-cancer properties (30, 31). It is reported to exert its cytotoxic effects through NAD(P)H:quinone oxidoreductase-1 (NQO1)-mediated redox cycling, generating reactive oxygen species (ROS) that cause DNA damage and necrosis (32-34). Preclinical studies revealed that  $\beta$ -lapachone preferentially targets NQO1-over-expressing tumors, including lung, breast, pancreatic, and prostate cancers (33-37).

$\beta$ -lapachone repressed growth of colorectal cancer cells through ferroptosis (38) and suppressed cervical cancer via interaction with AKT1 (39).  $\beta$ -lapachone was shown to induce apoptosis, inhibit proliferation, and enhance the efficacy of chemotherapeutic agents in cancer cells (40-43).  $\beta$ -lapachone has been evaluated in early-phase clinical trials. A phase I study (NCT00054977) in patients with advanced solid tumors determined the safety profile, pharmacokinetics, and maximum tolerated dose. Combined regimens with chemotherapy and radiation are being studied in preclinical

and clinical settings. Despite its potential anti-neoplastic effects,  $\beta$ -lapachone was not previously functionally validated as a USP18 inhibitor.

We report here that  $\beta$ -lapachone treatment statistically-significantly reduced proliferation and induced apoptosis in murine and human lung cancer cell lines. Engineered USP18 overexpression opposed these effects. *In vivo*  $\beta$ -lapachone treatment statistically-significantly repressed tumor growth in a human lung cancer cell line xenograft transplanted into immune-deficient mice.  $\beta$ -lapachone pharmacodynamically increased ROS levels, but its anti-neoplastic effects occurred at concentrations where ROS accumulation was hardly detected. Notably, ROS scavenger treatments did not prevent  $\beta$ -lapachone anti-cancer effects at these dosages. This indicated a mechanism other than ROS production was engaged by  $\beta$ -lapachone treatment.

An interferon-stimulated response element (ISRE) reporter assay found that  $\beta$ -lapachone activated JAK/STAT signaling, as expected for USP18 inhibition.  $\beta$ -lapachone treatment of lung cancer cells was found to enhance global ISGylation. RNA sequencing after  $\beta$ -lapachone treatment (as compared to controls) of lung cancer cells identified expressed genes and pathways preferentially regulated by  $\beta$ -lapachone treatment. The co-transfection of USP18 provided insights into the pathways regulated by USP18 inhibition via  $\beta$ -lapachone treatment. Proteomic analysis identified known and novel ISG15-conjugated proteins. That  $\beta$ -lapachone acts through specific USP18 residues and within a defined USP18 pocket was shown through computational modeling and functional analyses of mutant USP18 species.

In summary, the findings presented here establish  $\beta$ -lapachone as a previously unrecognized functional USP18 inhibitor and as a valuable tool for examining USP18-mediated oncogenic signaling.  $\beta$ -lapachone itself serves as a proof-of-concept tool compound for elucidation of future derivatives with even greater potency as USP18 inhibitors. The identification of  $\beta$ -lapachone as a USP18 inhibitor opens new ways to target USP18 in cancer or immune-based therapy.

## Results

### High-throughput screen identifies candidate USP18 inhibitors

To identify small molecule inhibitors of USP18, high-throughput screening was performed using a diverse compound library containing 79,493 small molecules, as shown in **Fig. 1A**. A fluorescence-based enzymatic assay was established using recombinant, enzymatically active USP18 protein as displayed in **Fig. 1B** and **C**. Purified USP18 displayed deISGylating activity, which was independently confirmed by immunoblot assays in **Fig. 1D**. Primary screening, followed by counter screening, identified 13 candidate inhibitors that were subjected to dose–response assays at various treatment durations (0 hour, 0.5 hour, 1 hour and 4 hours).

The strategy deployed in this screen is summarized in **Fig. 1E**. This approach progressed from high-throughput enzymatic assays through multiple biochemical, transcriptional, and cell-based assays. Five compounds displayed reproducible enzymatic inhibition against USP18 in concentration- and time-dependent manners. The increased inhibition observed with prolonged pretreatment suggests that these compounds may act via a non-instantaneous or potentially covalent mechanism, and

the detailed mechanism of action is under investigation. Among the five candidate inhibitors, three compounds ( $\beta$ -lapachone, 9,10-phenanthrenequinone and 2-nitrophenanthrene-9,10-dione) shared similar structural scaffolds and physicochemical properties, prompting further interest in their mode of action, as shown in **Fig. 1F**. Two of these five compounds did not appreciably suppress lung cancer cell proliferation and were not moved forward for further screening, as shown in **Supplementary Fig. 1**. The observation of similar scaffolds in the three most active USP18 inhibitors motivated the subsequent molecular modeling studies to investigate how these compounds, particularly  $\beta$ -lapachone, engaged USP18 at functional and structural levels.

$\beta$ -lapachone is reported to confer cytotoxic effects through NAD(P)H:quinone oxidoreductase-1 (NQO1)-mediated redox cycling, generating ROS that cause DNA damage and necrosis (32-34). Yet, the data displayed in **Fig. 1G** found that  $\beta$ -lapachone treatment generated negligible ROS at 1  $\mu$ M and 2.5  $\mu$ M concentrations. A marked increase in ROS was only observed at the higher dosage of  $\beta$ -lapachone 4  $\mu$ M, as measured by flow cytometry. Notably, combined treatment with the ROS scavenger N-acetylcysteine (NAC) substantially attenuated this ROS elevation, at the  $\beta$ -lapachone 4  $\mu$ M dosage, but hardly at the lower dosages as shown in **Fig. 1G**. These findings indicated that  $\beta$ -lapachone was activating anti-cancer mechanisms at concentrations lower than 4  $\mu$ M that did not engage ROS. Studies were next conducted to elucidate these mechanisms.

### **$\beta$ -lapachone treatment suppresses lung cancer cell proliferation**

Functional consequences of  $\beta$ -lapachone treatment were explored.  $\beta$ -lapachone statistically-significantly repressed proliferation of human lung cancer cell lines A549 and H1299 (**Fig. 2A**) in a dose-dependent manner.  $\beta$ -lapachone treatment augmented apoptosis in A549 and H1299 cells, as shown in **Fig. 2B**. This growth inhibition was not reversed by co-treatment with the ROS scavenger NAC, as seen in **Fig. 2C**. The  $\beta$ -lapachone treatment at 2.5 $\mu$ M concentrations also increased apoptosis in these cancer cells, but NAC co-treatment did not appreciably attenuate this response, as displayed in **Fig. 2C**. These results suggested that the antiproliferative and pro-apoptotic activities of  $\beta$ -lapachone occur at lower concentrations largely through an ROS-independent mechanism. In addition,  $\beta$ -lapachone suppressed proliferation and induced apoptosis of murine lung cancer 344SQ cells in a similar dose-dependent pattern as in human lung cancer cells, as shown in **Supplementary Fig. 2**.

To explore if these effects are mediated through USP18, USP18 rescue experiments were performed. Independently engineered gain of USP18 expression in human A549 and H1299 lung cancer cells antagonized  $\beta$ -lapachone-induced growth inhibition (**Fig. 2D**). This indicated that reduction of USP18 activity contributed to the antiproliferative signals of  $\beta$ -lapachone.

To confirm and extend these *in vitro* findings to the *in vivo* setting, human lung cancer xenograft models were interrogated using the H1299 lung cancer cell line. Oral administration of  $\beta$ -lapachone at the 12.5 mg/Kg and 25 mg/Kg of mouse body weight decreased lung tumor growth as compared to controls. The tumor growth decline at the 25 mg/Kg of mouse body weight reached statistical-significance versus vehicle controls, see **Fig. 2E**. Notably, this decline in lung cancer growth was associated with a

statistically significant reduction in proliferation as measured by Ki-67 staining and an increase in apoptosis TUNEL scoring, as displayed in **Fig. 2F**. These findings demonstrate that  $\beta$ -lapachone treatments (as compared to vehicle control treatments) confer anti-cancer effects in immune deficient mice harboring human lung cancer cells. Given these antineoplastic effects, it was next studied whether these actions were mediated through USP18 inhibition.

### **$\beta$ -lapachone antagonizes USP18-dependent activities**

To confirm target specificity, it was explored if  $\beta$ -lapachone treatment affected USP18-dependent signaling in A549 lung cancer cells. Consistent with an antagonist of USP18 function,  $\beta$ -lapachone treatment enhanced activity in a dose-dependent manner of the transfected interferon-stimulated response element (ISRE) reporter assay, as depicted in **Fig. 3A**. In contrast, engineered gain of human USP18 expression repressed this ISRE activity. This inhibited the increase in reported activity that was conferred by  $\beta$ -lapachone treatment. Consistent with these findings, immunoblot analysis demonstrated that  $\beta$ -lapachone treatment also increased global ISGylation in A549 human lung cells, as seen in **Fig. 3B**. Notably,  $\beta$ -lapachone treatment preferentially affected ISGylation given that this treatment had little impact on ubiquitin, SUMO-2/3, or NEDD8 conjugation other than a minor effect on SUMO-2/3 conjugation observed only at the highest  $\beta$ -lapachone examined treatment concentrations, as shown in **Fig. 3C** and **3D**.

### **Molecular modeling of $\beta$ -lapachone binding to a USP18**

To elucidate the molecular basis of USP18 inhibition by individual  $\beta$ -lapachone, 9,10-phenanthrenequinone, and 2-nitrophenanthrene-9,10-dione treatments, molecular modeling of the USP18–ISG15 interaction interface was performed. Intriguingly, structural analyses identified a hydrophobic pocket needed for substrate engagement. Within this pocket, the phenylalanine residue F259 was found to be a critical determinant of ligand binding. As shown in **Fig. 4A**, the conformation of F259 differs between ISG15-bound (interacting, red) and unbound (non-interacting, yellow) USP18, indicating its dynamic role in mediating substrate recognition. Additional modeling highlighted three residues—D139, F259, and T266—as key interaction points through which  $\beta$ -lapachone engages USP18 within this hydrophobic pocket (see **Fig. 4B**).

Consistent with these findings, docking analyses revealed the compounds having USP18 enzymatic inhibitory properties ( $\beta$ -lapachone, 9,10-phenanthrenequinone, and 2-nitrophenanthrene-9,10-dione) bound the identified USP18 pocket in a similar manner, as displayed in **Fig. 4C**. Binding energy calculations supported these findings, revealing favorable energetics for ligand engagement, with  $\beta$ -lapachone exhibiting a calculated binding energy of approximately -6.1 kcal/mol, comparable to those of 9,10-phenanthrenequinone, and 2-nitrophenanthrene-9,10-dione, as shown in **Fig. 4D**. These results provide a mechanistic basis through which  $\beta$ -lapachone and its analogs inhibit USP18 enzymatic activity through occupancy of a conserved hydrophobic binding pocket defined by residues D139, F259, and T266.

To independently validate these molecular modeling predictions, site-directed mutagenesis of the three critical amino acid residues (D139, F259, and T266) in USP18 was next performed. *In silico* energy calculations revealed that mutation of any of these

residues would markedly reduce the predicted binding affinity between  $\beta$ -lapachone and USP18, with the greatest loss of interaction observed in examination of the triple mutant (see **Fig. 5A** and **Supplemental Fig. 3**). Structural visualization confirmed that  $\beta$ -lapachone bound tightly to wild-type USP18 but did not similarly bind mutant USP18 proteins, consistent with loss of the hydrophobic-pocket interaction displayed in **Fig. 5B**.

To ensure proper protein expression, immunoblot analyses verified comparable expression levels of wild-type and mutant USP18 constructs in **Fig. 5C**. Functional testing using the interferon-stimulated response element (ISRE) reporter assay showed that Interferon treatment elevated the luciferase activity, while transfection of wild-type USP18 species into A549 lung cancer cells opposed this activation. In marked contrast, transfection of the triple mutant USP18 species did not appreciably affect this activation and indicated that the triple mutant USP18 species was no longer functional, as displayed in **Fig. 5D**. Together, these findings provide a mechanistic basis through which  $\beta$ -lapachone disrupts USP18 enzymatic activity by binding the hydrophobic pocket needed for ISG15 recognition (44).

Among the three highlighted USP18 candidate inhibitors,  $\beta$ -lapachone was prioritized for further pharmacodynamic studies because it exhibited the most robust inhibitory activity in enzymatic, biochemical, cellular, and tumorigenicity assays.  $\beta$ -lapachone is a natural product with known antineoplastic properties (35-37). It is a tool compound to further assess the consequences of USP18 inhibition.

### **Transcriptomic profiling and USP18-dependent $\beta$ -lapachone response**

RNAseq was next performed to determine transcriptional pathways engaged by  $\beta$ -lapachone treatment. This treatment of A549 lung cancer cells as compared to vehicle controls caused a distinct pattern of differentially expressed genes, including both up-regulated and down-regulated transcripts, as seen in **Fig. 6A** and **Supplementary Fig. 4A**. To determine whether these responses were mediated by USP18 inhibition, transcriptomes of USP18-overexpressing A549 lung cancer cells were compared to that of empty-vector controls treated with  $\beta$ -lapachone. Exogenous USP18 expression antagonized a subset of  $\beta$ -lapachone-induced transcriptional changes, indicating that the effects displayed in **Fig. 6B** and **Supplementary Fig. 4B** and **4C** are likely USP18-dependent.

Real-time PCR assays independently validated representative expressed genes that were either reduced (NR4A2, ENTPD1, DCC and USP41) or increased (FGF13, IL31RA, OTUD7A, and KLK2,) following  $\beta$ -lapachone treatment, as shown in **Fig. 6C**. To assess the translational relevance of these  $\beta$ -lapachone-regulated and USP18-dependent genes, transcriptomic and survival data were interrogated using The Cancer Genome Atlas (TCGA) lung adenocarcinoma cohort. High mRNA expression levels of USP18 or ISG15 were each associated with poorer overall lung cancer survival in **Fig. 6D**. The prognostic value of USP18 and ISG15 in lung squamous cell carcinoma is shown in **Supplementary Fig. 4D**. Among  $\beta$ -lapachone-suppressed genes whose expression was rescued by USP18 overexpression, including LINC00319, NCCRP1, and ENTPD1, higher expression in human lung adenocarcinomas was associated with unfavorable survival outcomes in **Fig. 6D**.

In contrast,  $\beta$ -lapachone–expressed genes that were antagonized by engineered USP18 over-expression, including FGF13, IL31RA, OTUD7A, and KLK2, showed the opposite survival patterns with higher expression levels in lung adenocarcinomas that were associated with an improved survival, as shown in **Fig. 6E**. These findings serve to identify USP18-dependent gene expression pathways that are engaged by  $\beta$ -lapachone treatment. To delineate species that could mediate the anti-neoplastic effects of  $\beta$ -lapachone, proteomic analyses were next done.

### **Proteomic analyses reveal $\beta$ -lapachone–regulated ISG15-related proteins**

To further define the consequences of USP18 inhibition, we performed ISG15 immunoprecipitation–mass spectrometry analyses in A549 lung cancer cells expressing an empty vector or a USP18-expressing vector. These transfectants were each treated with vehicle or  $\beta$ -lapachone at the 2.5 $\mu$ M concentration. Under stringent elution conditions designed to retain preferentially the covalently bound ISG15 conjugates,  $\beta$ -lapachone treatment substantially affected the ISG15-conjugated proteome. Comparison between  $\beta$ -lapachone–treated control cells and USP18-over-expressing A549 lung cancer transfectants identified proteins whose ISGylation were rescued by USP18 expression, as expected for effects that were USP18-dependent. Among the ISG15-conjugated proteins identified, 86 matched previously reported ISG15 targets, while 70 represented new candidate ISG15-conjugated proteins, as displayed in **Fig. 7A** and **Supplemental Fig. 5**. Pathway enrichment analysis revealed that these  $\beta$ -lapachone–regulated ISG15 substrates were distributed across multiple cellular

processes, including signal transduction, RNA and protein modification, mitochondrial transport, vesicle trafficking, and chromatin regulation, as shown in **Fig. 7B**.

The expression of a representative novel ISGylated protein, DYNLL1, was interrogated by immunoblot analyses following  $\beta$ -lapachone as compared to vehicle treatment. These findings are shown in **Fig. 7C** and reveal a  $\beta$ -lapachone dose-dependent repression of DYNLL1 immunoblot expression (quantification shown). To establish the translational relevance of this observation TCGA lung adenocarcinoma cohort was examined for the impact on survival of differential expression of DYNLL1. Intriguingly, a favorable survival outcome was observed in lung cancer cases having low as compared to high levels of DYNLL1 levels within the lung cancers. Other novel and previously recognized ISGylated species were examined for their associations for lung cancer survival in **Fig. 7D** and **7E**. Differential expression profiles of several identified ISG15-conjugated proteins were explored for their prognostic impact across different cancer types, as shown in **Supplementary Fig. 6**.

Several  $\beta$ -lapachone-upregulated ISG15 substrates, including DYNLL1, HAUS6, LAMB3, BANF1, EIF5A and ANXA2P2 showed statistically-significant associations with survival of cancer patients, as seen in **Fig. 7D**. Four previously unrecognized ISG15 targets (PCBP2, NME1, TUBA1C and TUBA4A) were confirmed as  $\beta$ -lapachone-regulated conjugates whose high expression profiles were associated with unfavorable survival outcomes in **Fig. 7E**. These observations broaden an understanding of  $\beta$ -lapachone treatment effects on the ISGylated proteome.

## **Discussion**

Lung cancer is the leading cause of cancer mortality and new therapeutic strategies are needed to improve clinical outcomes (1). Recent studies highlighted the deISGylation enzyme USP18 as an emerging antineoplastic target, due to its central role in regulating type I interferon signaling through deISGylation from substrate proteins (3-9, 20-23). That prior work indicated that USP18-mediated de-ISGylation can stabilize multiple proteins involved in immune modulation as well as those affecting cancer cell survival, proliferation, and tumorigenicity.

Building upon this previous work, this study identified and characterized USP18 inhibitors that exhibit anti-neoplastic effects. Of these compounds,  $\beta$ -lapachone was found to be a small-molecule USP18 antagonist that exhibited the most prominent anti-neoplastic properties in lung cancer models in *in vitro* and *in vivo* assays. Pharmacological USP18 inhibitors with anti-neoplastic activity are not yet reported having functional anti-cancer validation. That is why this study addresses a prior knowledge gap in cancer research.

A high-throughput screen of ~80,000 small-molecule compounds assessed enzymatically active recombinant human USP18 to identify potential small molecule inhibitors. These studies yielded 42 candidate compounds with USP18 inhibitory activity. To explore further the USP18 inhibitory effects of these compounds, cell-based and lung cancer xenograft assays were performed along with transactivation, transcriptional, and proteomic assays. Three compounds emerged from these studies as candidates exhibiting the most USP18 inhibitory activities.

Molecular docking and modeling analyses revealed that all three highlighted compounds were bound to the same hydrophobic pocket of USP18 protein. This is

consistent with previous structural studies that revealed this pocket mediated USP18's interaction with ISG15 (44). Interestingly, all three compounds showed structural convergence. Two of these three compounds shared a similar structural backbone. These findings indicated a common pharmacophore. This provides a basis for future structure-guided compound optimization. Supporting this interpretation were studies performed in **Fig. 4** and **Fig. 5** that showed that based on modeling studies a mutated form of USP18 was engineered to no longer bind to  $\beta$ -lapachone. As expected, this delISGylase did not function as did the wild-type USP18 species in interferon transactivation assays in **Fig. 5D**. Prior work compared the relationship between the enzymatic and scaffolding properties of USP18 species (45). Perhaps  $\beta$ -lapachone binding to USP18 elicited conformational changes within human USP18 protein that affected the ISRE reporter assay results reported here.

The high hydrophobicity of these candidate compounds made conduct of biophysical ligand–protein binding assays difficult to perform. This is why studies reported here relied on molecular docking and modeling to infer binding interactions. Future work should identify optimal lead compounds to generate drug-like USP18 inhibitors. Those studies would be facilitated by *in silico* modeling studies as presented here that could accelerate this development.

Functional studies that were performed in lung cancer cells demonstrated that  $\beta$ -lapachone exhibited prominent USP18-inhibitory activity. Treatment with  $\beta$ -lapachone increased global ISGylation and activated ISRE reporters, consistent with loss of USP18-mediated delISGylation. It was thus not surprising that co-transfection of wild-type but not the mutant form of USP18 that lacked the ability to sustain this binding

pocket antagonized the activity of  $\beta$ -lapachone. These  $\beta$ -lapachone anti-neoplastic effects were associated with reduced cell proliferation and increased apoptosis in both human and murine lung cancer cells. Engineered over-expression of wild-type but not triple mutant USP18 species antagonized  $\beta$ -lapachone effects. These findings are consistent with the antineoplastic activity of  $\beta$ -lapachone engaging the enzymatic activity of USP18.

One hypothesized feature of the  $\beta$ -lapachone mechanism of action is its ability to generate reactive oxygen species (ROS) via NQO1-mediated redox cycling (32). It is notable that the data presented in **Fig. 1** and **Fig. 2** showed that effective dosages of  $\beta$ -lapachone that yielded prominent anti-cancer effects produced minimal ROS levels. Likewise, treatment with ROS scavengers did not appreciably reverse the observed  $\beta$ -lapachone anti-neoplastic signals that were observed at dosages lower than  $4\mu\text{M}$ . These findings indicated that  $\beta$ -lapachone can act through USP18 inhibition in the experiments performed here, rather than via ROS-dependent mechanisms, as expected if NQO1-mediated redox cycling were prominently engaged at this dosage. Future structural modification or optimization of  $\beta$ -lapachone analogs should aim to enhance USP18 specificity while minimizing ROS-inducing activity to improve selectivity and therapeutic anti-cancer properties.

Prominent *in vivo* anti-tumor activity of  $\beta$ -lapachone was observed. Treatment of the H1299 xenograft lung cancer model led to statistically-significant lung cancer growth inhibition in this *in vivo* model, as shown in **Fig. 2**. This anti-neoplastic effect was associated with a decrease in proliferation and an increase in apoptosis markers within  $\beta$ -lapachone-treated lung tumor bearing mice. These findings confirm and extend prior

work showing statistically significant *in vivo* anti-cancer effects of  $\beta$ -lapachone treatment of A549 lung cancer xenografts as well as in other *in vivo* cancer xenograft models (37, 38, 43, 46). These studies provide a therapeutic rationale for targeting USP18 in lung or other cancers that over-express USP18 relative to the histopathologically normal lung (23). That  $\beta$ -lapachone treatment acts at least partly by altering interferon signaling was consistent with the transcriptomic and proteomic analyses displayed in **Fig 6** and **Fig. 7**. Those studies revealed that  $\beta$ -lapachone can upregulate interferon-stimulated genes and broaden the repertoire of ISGylated proteins, including previously unrecognized ISG15 substrates.

These results indicate that the ISG15/USP18 axis could regulate broader cellular pathways than previously reported. Identification of these previously unrecognized ISGylated targets should elucidate novel proteins that are engaged by this post-translational modification and that would elicit anti-tumorigenic effects. Likewise, these species might inform translationally-relevant biomarker development following USP18 antagonism.

Beyond its role in regulating ISGylation and interferon signaling, USP18 has additional interferon-independent functions that may contribute to cancer biology and influence therapeutic responses (17). The transcriptomic and proteomic changes observed following  $\beta$ -lapachone treatment were not limited to canonical interferon-stimulated genes, but also involved pathways linked to signal transduction, metabolism, vesicle trafficking, and protein regulation, indicating that USP18 inhibition can affect multiple cellular processes. These broader effects suggest that pharmacologic targeting of USP18 may have consequences that extend beyond interferon pathway modulation.

At the same time, USP18 plays an important role in immune regulation, and its inhibition could influence immune responses depending on cellular and tissue context. While the present study focused on tumor-intrinsic effects using immune-deficient xenograft models, future studies in immunocompetent systems will be necessary to define the immune consequences and therapeutic window of USP18 inhibition.

The findings presented here establish  $\beta$ -lapachone as a USP18 inhibitor. Yet,  $\beta$ -lapachone is at best a tool compound and not yet a clinical lead, given its off-target activities or drug-like properties. The structural convergence of the three most active USP18 inhibitors described here provides a rationale for the future discovery of a clinical lead compound. These studies should aim to develop derivatives of  $\beta$ -lapachone or other promising compounds with related scaffolds that can interact with the USP18 pocket described here and have optimal selectivity, potency, and formulation needed for a promising clinical lead.

In summary, this study found that  $\beta$ -lapachone antagonizes USP18 anti-neoplastic activity. This reduced proliferation, increased apoptosis and augmented ISGylation. Collectively, this led to repressed human lung cancer growth in mice as in **Fig. 2** and in lung and other *in vivo* cancer models that were reported by others (37, 38, 43, 45). Anti-cancer function of a USP18 inhibitor is just one aspect of the actions of USP18 (19-29). USP18 also plays a role in regulation of interferon signaling and viral infections (17-19). Thus, any USP18 inhibitor would likely have therapeutic properties beyond its anti-neoplastic activity.

Prior studies revealed that USP18 is an appealing antineoplastic target (19-29). The studies presented here indicate that  $\beta$ -lapachone elicits substantial inhibition of USP18

activity. This finding, coupled with the USP18 pocket through which  $\beta$ -lapachone and other USP18 antagonists bind, provide avenues to develop more effective inhibitors in future work. The USP18 inhibitory compounds described here will help develop future USP18 inhibitors with desired drug-like properties. Such compounds that exhibit enhanced USP18 expression could enter clinical trial testing for lung and likely other cancers.

## **Methods**

### **Sex as a biological variable**

This study examined antineoplastic effects of  $\beta$ -lapachone in female NSG mice as recipients for H1299 lung cancer xenografts because female recipient mice typically exhibit less aggressive behaviors than do male mice. Studies performed in xenograft lung tumors did not reveal an appreciable difference in anti-tumor responses to  $\beta$ -lapachone observed between male and female recipient mice (40-43).

### **Compound libraries**

A diverse library of 79,493 small-molecule compounds was screened. This library comprised fragment sets (18,037 compounds, Chembridge, San Diego, CA and Chemdiv, San Diego, CA), kinase sets (11,240 compounds), Chembridge, San Diego, CA), diversity sets (42,957 compounds) from the National Cancer Institute, Chemdiv, San Diego, CA, LifeChem, Canada, and Maybridge/ThermoFisher Scientific, Waltham, MA), biologically annotated compounds (5,175 compounds), and those from an

academic collection (2,000 unique molecules, University of Texas at Austin and University of Kansas). Compounds were dissolved in dimethyl sulfoxide (DMSO) at 10mM concentrations, placed into 384-well plates, and stored at -40°C.

### **Screening for USP18 inhibitors and validation**

A biochemical assay monitoring the deISGylation activity of USP18 was performed using the fluorogenic substrate 7-amido-4-methylcoumarin (AMC) labeled ISG15 (#UL-553, Bio-technie, Minneapolis, MN) and was deployed as a high-throughput small molecule screening and hit characterization (47). Primary screening was conducted at 50 $\mu$ M compound concentrations following this procedure: 5 $\mu$ L of enzyme mixture containing 2X USP18 in 1X assay buffer (50 mM HEPES pH 7.5, 10 mM DTT, 5% v/v glycerol, 0.01% (v/v) Tween-20, and 0.1% (w/v) BSA) or 1X buffer only were dispensed to 384-well assay plates (#262260, Thermo Fisher Scientific, Waltham, MA). Using 50nL of compounds (Columns 3-22) or 100% DMSO (columns 1,2,23 and 24) were dispensed to assay plates and incubated for 1 hour at room temperature. Then 5 $\mu$ L of 2X ISG15-AMC in 1X buffer was added to start the reaction. The reaction at room temperature was quenched after 1 hour by adding 5 $\mu$ L of 0.1N HCl. The fluorescence intensity at excitation/emission wavelengths of 360  $\pm$  20nm/450  $\pm$  20nm was read on a Synergy H4 multifunctional plate reader (Agilent, Santa Clara, CA). Final concentrations of mUSP18 and ISG15-AMC were 25nM and 600nM, respectively. Fluorescence interference was assessed on primary hits using the following control. An AMC-only counter screen was performed in which hit compounds (50 $\mu$ M) were incubated with free AMC fluorophore (600nM) in the absence of enzyme under matched buffer/DMSO

conditions, and fluorescence was measured at Ex/Em 360/450nm. Compounds that reduced the AMC signal by more than 30% were deprioritized.

A dose-response inhibition of each compound was examined using the same biochemical assay. Compounds at various concentrations, starting from 50 $\mu$ M and serially diluted eight times, were tested. IC<sub>50</sub> values were calculated using a four-parameter logistic curve fit. To investigate the time-dependent inhibition kinetics, compounds were pre-incubated with the described human USP18 enzyme at various time points (0, 0.5, 1, and 4 hours) before the addition of the substrate and at varying concentrations. An additional control was applied to the most promising hits in this study. An endpoint spike control was performed, in which USP18 reactions were run to the assay endpoint and quenched, as described. After that, compounds were added, and fluorescence was re-read to assess post-reaction quenching/inner-filter effects.

## **Computational Modeling**

AlphaFold 3 (48) was used to predict the structures of human USP18 and the USP18-ISG15 complex. Protein-ligand binding free energies were computed using the VeraChem Mining minima (VM2) method (49-53) utilizing the ff14SB (54) and GAFF2 (55) force fields for USP18 and ligand, respectively. For the VM2 computations, parameters were modified from default values, as follows: live/real = 8/6 Å, protein-ligand conformer search style = “vrigorous,” protein-ligand number of search steps = 1000.

Molecular dynamics (MD) simulations were performed using Amber 22 (56) with the ff19SB (57), GAFF2 (55), and 12-6 LJ nonbonded (58) force fields for protein, ligand,

and Zn<sup>2+</sup>, respectively. Following VM2 protein-ligand minimizations, complexes were placed in a cuboid box with boundary of 12 Å, solvated with Optimal Point Charge (OPC) waters (59), neutralized with a Cl<sup>-</sup>, and additional Na<sup>+</sup>/Cl<sup>-</sup> ions added to mimic salt concentration of 0.15M. MD runs were performed over 2fs time steps while constraining all hydrogen bonds via the Systematic Hard-Sphere Adjustment of Kinetic Energy (SHAKE) algorithm. A temperature of 300K and pressure of 1Pa in constant number of particles, pressure, and temperature (NPT) simulations were maintained using the Berendsen thermostat and Berendsen algorithm (60). A cutoff of 9 Å was applied to non-bonded interactions and explicit solvent periodic conditions were used.

For each simulation an initial multi-step equilibration process was performed starting with solvent treatment only (solute heavy atom restraint = 100): energy minimization, short period of heating from 100K to 300K (40ps), and short MD at 300K (50ps). The complete system was then minimized and MD performed for 100ps where both simulations used solute heavy atom constraint = 25. Next, several energy minimizations were performed with decreasing solute restraint (20, 15, 10, 5, 2.5, 1.0, 0.1, 0.01, and 0), then heating from 100 to 300K (1 fs/Cα restraint = 10) followed by several MD runs at 300 K with varying times/restraints: 3 fs/Cα restraint = 1, 4 fs/Cα restraint = 0.1, 5 fs/no restraints. Lastly, production (unrestrained) MD runs were performed for 1μs and these trajectories were analyzed using the cpptraj module.

Computation of the initial protein-ligand VM2 binding energy was started from a structure in which the ligand was placed in the hydrophobic pocket of USP18 above the F259 residue. Computation of the post-MD VM2 binding energy was started from the

final MD structure (1 $\mu$ s). PyMOL was used for mutagenesis and structure illustrations (61).

## **Cell culture**

Human (H1299 and A549) and murine (344SQ) lung cancer cell lines were cultured in RPMI-1640 medium (#11875093, Thermo Fisher Scientific, Waltham, MA) supplemented with 10% fetal bovine serum (FBS, #A5256701, Thermo Fisher Scientific, Waltham, MA). Cells were cultured at 37°C in a humidified incubator with 5% CO<sub>2</sub>. The 344SQ murine lung cancer cell line was provided by Dr. Jonathan M. Kurie (MD Anderson Cancer Center, Houston, TX). Human lung cancer cell lines H1299 and A549 were purchased and authenticated by American Type Culture Collection (ATCC).

## **Small interfering RNAs and transfection**

Independent transient transfections of A549, H1299 and 344SQ lung cancer cells were with small interfering RNAs (siRNAs) following the manufacturer's methods for siRNA-mediated transfection experiments (Dharmacon, Lafayette, CO) (29). Independent siRNAs to target USP18 and inactive control siRNAs were purchased (Dharmacon, Lafayette, CO); siRNAs that targeted USP18 were: USP18 human siRNA3 (5'-GGACUACCCUCAUGGCCUG-3'); and USP18 human siRNA4 (5'-GCAAUCUGUCAGUCCAUC-3'). Transfection efficiency was measured by co-transfecting the siGLO Red Transfection Indicator (Dharmacon, Lafayette, CO).

## **Immunoblot assays**

Cells were lysed with ice-cold Pierce RIPA Lysis and Extraction Buffer (#89900, ThermoFisher Scientific, Waltham, MA) supplemented with Halt Protease and Phosphatase Inhibitor Cocktail (#78440, ThermoFisher Scientific, Waltham, MA). Proteins were resolved by SDS-PAGE before transfer to Trans-Blot Turbo Mini 0.2 $\mu$ m PVDF Transfer Packs (#1704156, Bio-RAD, Hercules, CA). Membranes were blocked with 5% nonfat milk in Tris-buffered saline (#1706404XTU, Bio-RAD, Hercules, CA) and with 0.1% Tween-20 (#170653, Bio-RAD, Hercules, CA) (TBS-T) solution for at least 1 hour before overnight incubation at 4°C with a primary antibody diluted in 1% nonfat milk or 1% BSA in TBS-T. This was followed by 10-minute washes x 3 in TBS-T solution and with a 1-hour incubation with the desired secondary antibody diluted in 5% nonfat milk. After three additional washes, antibody binding was visualized by Clarity Western ECL Substrate (#1705061, Bio-RAD, Hercules, CA) and quantified by Image Lab software (Bio-RAD, Hercules, CA).

Anti-ISG15 antibody was provided by Dr. Shyamal Desai at the Department of Biochemistry and Molecular Biology, Louisiana State University Health Sciences Center - School of Medicine, New Orleans (62). Primary antibodies were: Vinculin (#V4505, Millipore Sigma, Burlington, MA), GAPDH (#14C10, Cell Signaling Technology, Danvers, MA) and  $\beta$ -Actin (#4967, Cell Signaling Technology, Danvers, MA). Secondary goat anti-mouse IgG (#1706515, Bio-RAD, Hercules, CA) and goat anti-rabbit IgG (#1706516, Bio-RAD, Hercules, CA) were used. Immunoblots were stripped using Restore PLUS Western Blot Stripping Buffer (#46430, Thermo Fisher Scientific, Waltham, MA) followed by TBS-T solution washing.

### **Proliferation assays**

Logarithmically-growing cells were seeded at optimized densities for each examined lung cancer cell line and cells were plated onto individual wells of 12-well tissue culture dishes, in triplicate. Cells were treated with  $\beta$ -lapachone at varying dosages and independently with the vehicle (DMSO) as a control 24 hours later. Proliferation was measured using the WST-1 assay (#5015944001, Millipore Sigma, Burlington, MA) after 24-72 hours of the indicated compound exposures on the FLUOstar Omega microplate reader (BMG Labtech, Cary, NC). Proliferation studies were independently replicated at least three times.

### **Apoptosis assays**

Logarithmically-growing cells were seeded at optimized densities for each examined lung cancer cell line and cells were plated onto individual wells of 6-well tissue culture plates. Cells were treated with  $\beta$ -lapachone and independently with other candidate USP18 inhibitors at varying dosages and separately with vehicle (DMSO) 24 hours later. Apoptosis assays were performed using the FITC Annexin V Apoptosis Detection Kit (BioLegend, San Diego, CA) after 48 hours of drug exposure on a CytoFLEX flow cytometer (Beckman Coulter, Brea, CA). Independent triplicate replicate experiments were performed.

### **Reactive oxidative species (ROS) assays**

ROS production was measured using the Total Reactive Oxygen Species (ROS) Assay Kit 520 nm (#88-5930, ThermoFisher Scientific, Waltham, MA). Briefly, cells were

seeded at optimized densities into individual wells of 12 well tissue culture plates in triplicate, then treated with  $\beta$ -lapachone and independently with other USP18 candidate inhibitors at the indicated concentrations and durations as well as with the vehicle (DMSO) as a control. Cells were incubated with ROS assay stain solution 60 minutes prior to analysis on the CytoFLEX flow cytometer (Beckman Coulter, Brea, CA). The ROS scavenger N-acetylcysteine (NAC) (#A7250, Millipore Sigma, Burlington, MA) was used to interrogate ROS-dependent effects.

### **IFN reporter assays**

Cells were seeded onto individual wells of 96-well tissue culture plates in triplicate 24 hours before transfection using the ISRE Reporter Kit (#60613, BPS Bioscience, San Diego, CA) and jetPRIME transfection reagent (#55-134, Genesee Scientific, El Cajon, CA) following the manufacturer's protocol. Cells were then treated with  $\beta$ -lapachone and independently with other candidate USP18 inhibitors at varying concentrations. Results were compared to vehicle controls. Firefly and Renilla luciferase signals were measured using the TWO-Step Luciferase Assay System (#60683, BPS Bioscience, San Diego, CA) and using the FLUOstar Omega microplate reader (BMG Labtech, Cary, NC). The ratios of firefly luminescence signals to the corresponding Renilla luminescence signals were presented. The effects of co-transfection of wild-type as compared to mutant human USP18 species were explored.

### **RNA-seq analysis**

The A549 lung cancer cell line was engineered with an insertless control vector or with a USP18 expression vector and transfectants were independently treated with vehicle (DMSO) or with  $\beta$ -lapachone at indicated dosages before harvesting transfectants after 48 hours of these treatments. Comparisons were made to RNA-seq analysis performed in parental A549 lung cancer cells treated with  $\beta$ -lapachone at indicated dosages versus vehicle as a control. Total RNA was purified using the RNeasy Plus Universal Kit (#73404, Qiagen, Germantown, MD). The Illumina Stranded Total RNA library preparation ligation with RiboZero plus (#20040526, Illumina, San Diego, CA) was used for RNA sequencing. Ribosomal RNA (rRNA) was removed using biotinylated target-specific oligos with the Ribo-Zero Plus rRNA Depletion Kit (#20037135, Illumina, Illumina, San Diego, CA).

RNA was fragmented and used to generate first strand cDNA using reverse transcriptase and random primers, followed by second strand cDNA synthesis using DNA Polymerase I and RNase H. The resulting double-strand cDNA was used as the input to a standard Illumina library preparation with end-repair, adapter ligation, and PCR amplification to yield a library for sequencing. The final purified product was quantitated by qPCR assays before cluster generation and sequencing on NextSeq 2000 P2 flowcell (Illumina, Illumina, San Diego, CA) for paired end 100 cycle sequencing.

The Illumina bcl2fastq (version 2.20) was used to demultiplex and convert binary base calls and qualities to the fastq format. The sequencing reads were trimmed to remove adapters and low-quality bases using Cutadapt (version 1.18). The trimmed reads were mapped to the human reference genome (hg38) and GENCODE annotation

v30. The mapping was done using STAR aligner (version 2.7.0f) and with a two-pass alignment option. RSEM (version 1.3.3) for gene and transcript quantification was based on the GENCODE M21 GTF file. To identify differentially expressed genes (DEGs), DESeq2 (version 1.44.0) was used. Volcano plots were generated using EnhancedVolcano (<https://github.com/kevinblighe/EnhancedVolcano>). Heatmap plots were generated using pheatmap (<https://github.com/raivokolde/pheatmap>). DEGs were scored using these criteria: adjusted P value < 0.05 and fold change log<sub>2</sub>FC > 1. The statistically-significant DEGs were analyzed using Metacore software (version 24.1, <https://clarivate.com/products/metacore/>) to perform pathway enrichment analyses and to generate pathway maps.

### **Quantitative real-time reverse transcription polymerase chain reaction assays**

Quantitative real-time (RT) reverse transcription PCR (qRT-PCR) assays were performed in triplicate, as previously described (63). The respective primers used were purchased from Thermo Fisher Scientific (Waltham, MA): human KLK2 primer (Hs00428384\_g1); human IL31RA primer (Hs00371172\_m1); human OTUD7A primer (Hs00370128\_m1); human WASF3 primer (Hs00903488\_m1); human NR4A2 primer (Hs01117527\_g1); human DCC primer (Hs00180437\_m1); human ATP6V1B1 primer (Hs00266092\_m1); human USP41 primer (Hs02596851\_gH); human PARP8 primer (Hs01065404\_m1); human FGF13 primer (Hs00182807\_m1); human ALDH1L1 primer (Hs01003842\_m1); human ENTPD1 primer (Hs00969556\_m1); human  $\beta$ -Actin primer (Hs01060665\_g1), and human USP18 primer (Hs00276441\_m1).

## **TCGA survival analysis**

Survival analyses were performed using the Kaplan–Meier Plotter (<https://kmplot.com/analysis/>), which integrates gene expression and clinical outcome data from The Cancer Genome Atlas (TCGA) pan-cancer cohort. For each indicated cancer type, patient datasets were analyzed independently within the corresponding TCGA cohort. Patients were stratified into high- and low-expression groups based on the median mRNA expression value of the gene of interest, applied as a predefined cutoff to avoid bias from data-driven or optimized threshold selection. Overall survival was evaluated using Kaplan–Meier estimates, and statistical significance was determined using the log-rank test.

## **Statistical analysis**

Statistical analyses were done with the SPSS Statistics software (version 23, SPSS) and with GraphPad Prism software (version 8, GraphPad Software). Data were displayed as the mean and with Standard Deviations (SDs). Two-tailed Student's t tests compared differences between study groups with a P-value below 0.05 deemed statistically significant. Bonferroni corrections were used for multiple comparisons. Results of independent experiments were pooled to assess statistical significance. Experiments were typically performed in triplicate with at least three independent biological replicate experiments.

## **Lung cancer xenografts and drug treatments**

Human adenocarcinoma lung cancer H1299 cells ( $5 \times 10^6$  cells) were injected subcutaneously into female NSG mice (Charles River Laboratories, Wilmington, MA). These inbred mice were at least 8 weeks old and had at least a one-week acclimation period before experiments began. Mice with palpable tumors were randomized based on similar basal tumor sizes to receive oral doses of vehicle,  $\beta$ -lapachone (25 mg/kg body weight; 5 days per week) or  $\beta$ -lapachone (12.5 mg/kg body weight; 5 days per week). There were 10 tumor-bearing mice in each arm.  $\beta$ -lapachone was formulated in 2.5% DMSO/30% PEG400/67.5% Phosal MCT53 solution and treatment results were compared to that of vehicle-treated mice. Body weights and tumor volumes were measured three times weekly. Tumor volumes were calculated as  $V = (\text{length} \times \text{width}^2)/2$ . Hematoxylin and eosin staining of lung cancers as well as Ki-67 staining for proliferation and the TUNEL assay for scoring of apoptosis were performed as previously described (64).

### **Author contributions**

E.D. and Xi. Liu. conceived the study design, supervised the study, and interpreted the data. S.D.D. and G.G.P. provided key reagents. K.D., B.O., S.C.O., E.J.C., B.L., and G.G.P. interpreted the data. B.O., S.C.O., E.J.C., L.T-M., Z.C., Xiuxia L., B.L., Y.A., A.K.D. and R.M.S. collected data. J.I. and B. L. performed modeling studies. Xi Liu, B.O, K.D. and E.D. wrote this manuscript.

### **Funding support**

This work was supported by the NCI Intramural Research Program and Center for Cancer Research, NCI, and NIH contract #75N91019D00024 (ED), partly by the Frederick National Laboratory Research Support Program (XL and BL), a grant from the Samuel Waxman Cancer Research Foundation (ED), and by an American Cancer Society Professorship (ED), The Cancer Prevention and Research Institute of Texas (CPRIT) grant RP210088 (KD).

### **Study Approval**

All methods were performed and reported in accordance with Animal Research: Reporting of In Vivo Experiments (ARRIVE) guidelines (<https://arriveguidelines.org>). Animal experiments were approved by the National Cancer Institute (NCI) Animal Care and Use Committee (ACUC).

### **Data availability**

The datasets used as well as analyzed for this study will be available from the corresponding author upon reasonable request. The RNA seq data are available at the Gene Expression Omnibus accession GSE318135 (<https://www.ncbi.nlm.nih.gov/geo/query/acc.cgi?acc=GSE318135>). Supporting data value files are available as supplementary material.

### **Reference**

1. Siegel RL, Miller KD, Wagle NS, and Jemal A. Cancer statistics, 2023. *CA Cancer J Clin.* 2023;73(1):17-48.
2. Cho YJ, Cho YM, Kim SH, Shin KH, Jung ST, and Kim HS. Clinical analysis of patients with skeletal metastasis of lung cancer. *BMC Cancer.* 2019;19(1):303.
3. Ciechanover A. The ubiquitin-proteasome proteolytic pathway. *Cell.* 1994;79(1):13-21.
4. Popovic D, Vucic D, and Dikic I. Ubiquitination in disease pathogenesis and treatment. *Nat Med.* 2014;20(11):1242-53.
5. D'Cunha J, Knight E, Jr., Haas AL, Truitt RL, and Borden EC. Immunoregulatory properties of ISG15, an interferon-induced cytokine. *Proc Natl Acad Sci U S A.* 1996;93(1):211-5.
6. D'Cunha J, Ramanujam S, Wagner RJ, Witt PL, Knight E, Jr., and Borden EC. In vitro and in vivo secretion of human ISG15, an IFN-induced immunomodulatory cytokine. *J Immunol.* 1996;157(9):4100-8.
7. Kitareewan S, Pitha-Rowe I, Sekula D, Lowrey CH, Nemeth MJ, Golub TR, et al. UBE1L is a retinoid target that triggers PML/RARalpha degradation and apoptosis in acute promyelocytic leukemia. *Proc Natl Acad Sci U S A.* 2002;99(6):3806-11.
8. Pitha-Rowe I, Hassel BA, and Dmitrovsky E. Involvement of UBE1L in ISG15 conjugation during retinoid-induced differentiation of acute promyelocytic leukemia. *J Biol Chem.* 2004;279(18):18178-87.

9. Pitha-Rowe I, Petty WJ, Feng Q, Koza-Taylor PH, Dimattia DA, Pinder L, et al. Microarray analyses uncover UBE1L as a candidate target gene for lung cancer chemoprevention. *Cancer Res.* 2004;64(21):8109-15.
10. Zhao C, Beaudenon SL, Kelley ML, Waddell MB, Yuan W, Schulman BA, et al. The Ubch8 ubiquitin E2 enzyme is also the E2 enzyme for ISG15, an IFN-alpha/beta-induced ubiquitin-like protein. *Proc Natl Acad Sci U S A.* 2004;101(20):7578-82.
11. Arimoto K, Konishi H, and Shimotohno K. Ubch8 regulates ubiquitin and ISG15 conjugation to RIG-I. *Mol Immunol.* 2008;45(4):1078-84.
12. Dastur A, Beaudenon S, Kelley M, Krug RM, and Huibregtse JM. Herc5, an interferon-induced HECT E3 enzyme, is required for conjugation of ISG15 in human cells. *J Biol Chem.* 2006;281(7):4334-8.
13. Shi HX, Yang K, Liu X, Liu XY, Wei B, Shan YF, et al. Positive regulation of interferon regulatory factor 3 activation by Herc5 via ISG15 modification. *Mol Cell Biol.* 2010;30(10):2424-36.
14. Liu LQ, Ilaria R, Jr., Kingsley PD, Iwama A, van Etten RA, Palis J, et al. A novel ubiquitin-specific protease, UBP43, cloned from leukemia fusion protein AML1-ETO-expressing mice, functions in hematopoietic cell differentiation. *Mol Cell Biol.* 1999;19(4):3029-38.
15. Malakhov MP, Malakhova OA, Kim KI, Ritchie KJ, and Zhang DE. UBP43 (USP18) specifically removes ISG15 from conjugated proteins. *J Biol Chem.* 2002;277(12):9976-81.

16. Malakhova O, Malakhov M, Hetherington C, and Zhang DE. Lipopolysaccharide activates the expression of ISG15-specific protease UBP43 via interferon regulatory factor 3. *J Biol Chem*. 2002;277(17):14703-11.
17. Honke N, Shaabani N, Zhang DE, Hardt C, and Lang KS. Multiple functions of USP18. *Cell Death Dis*. 2016;7(11):e2444.
18. Potu H, Sgorbissa A, and Brancolini C. Identification of USP18 as an important regulator of the susceptibility to IFN-alpha and drug-induced apoptosis. *Cancer Res*. 2010;70(2):655-65.
19. Yan M, Luo JK, Ritchie KJ, Sakai I, Takeuchi K, Ren R, et al. Ubp43 regulates BCR-ABL leukemogenesis via the type 1 interferon receptor signaling. *Blood*. 2007;110(1):305-12.
20. Guo Y, Dolinko AV, Chinyenetere F, Stanton B, Bomberger JM, Demidenko E, et al. Blockade of the ubiquitin protease UBP43 destabilizes transcription factor PML/RARalpha and inhibits the growth of acute promyelocytic leukemia. *Cancer Res*. 2010;70(23):9875-85.
21. Guo Y, Chinyenetere F, Dolinko AV, Lopez-Aguiar A, Lu Y, Galimberti F, et al. Evidence for the ubiquitin protease UBP43 as an antineoplastic target. *Mol Cancer Ther*. 2012;11(9):1968-77.
22. Mustachio LM, Lu Y, Tafe LJ, Memoli V, Rodriguez-Canales J, Mino B, et al. Deubiquitinase USP18 loss mislocalizes and destabilizes KRAS in lung cancer. *Mol Cancer Res*. 2017;15(7):905-14.

23. Mustachio LM, Lu Y, Kawakami M, Roszik J, Freemantle SJ, Liu X, et al. Evidence for the ISG15-specific deubiquitinase USP18 as an antineoplastic Target. *Cancer Res.* 2018;78(3):587-92.
24. Cai X, Feng S, Zhang J, Qiu W, Qian M, and Wang Y. USP18 deubiquitinates and stabilizes Twist1 to promote epithelial-mesenchymal transition in glioblastoma cells. *Am J Cancer Res.* 2020;10(4):1156-69.
25. Diao W, Guo Q, Zhu C, Song Y, Feng H, Cao Y, et al. USP18 promotes cell proliferation and suppressed apoptosis in cervical cancer cells via activating AKT signaling pathway. *BMC Cancer.* 2020;20(1):741.
26. Feng L, Wang K, Tang P, Chen S, Liu T, Lei J, et al. Deubiquitinase USP18 promotes the progression of pancreatic cancer via enhancing the Notch1-c-Myc axis. *Aging (Albany NY).* 2020;12(19):19273-92.
27. Huang F, Zheng C, Huang L, Lin C, and Wang J. USP18 directly regulates Snail1 protein through ubiquitination pathway in colorectal cancer. *Cancer Cell Int.* 2020;20:346.
28. Liu X, Lu Y, Chen Z, Liu X, Hu W, Zheng L, et al. The ubiquitin-specific peptidase USP18 promotes lipolysis, fatty acid oxidation, and lung cancer growth. *Mol Cancer Res.* 2021;19(4):667-77.
29. Chen Z, Zheng L, Chen Y, Liu X, Kawakami M, Mustachio LM, et al. Loss of ubiquitin-specific peptidase 18 destabilizes 14-3-3zeta protein and represses lung cancer metastasis. *Cancer Biol Ther.* 2022;23(1):265-80.

30. Docampo R, Lopes JN, Cruz FS, and Souza W. Trypanosoma cruzi: ultrastructural and metabolic alterations of epimastigotes by beta-lapachone. *Exp Parasitol.* 1977;42(1):142-9.
31. Boveris A, Docampo R, Turrens JF, and Stoppani AO. Effect of beta-lapachone on superoxide anion and hydrogen peroxide production in Trypanosoma cruzi. *Biochem J.* 1978;175(2):431-9.
32. Gong Q, Hu J, Wang P, Li X, and Zhang X. A comprehensive review on beta-lapachone: Mechanisms, structural modifications, and therapeutic potentials. *Eur J Med Chem.* 2021;210:112962.
33. Yang Y, Zhou X, Xu M, Piao J, Zhang Y, Lin Z, et al. beta-lapachone suppresses tumour progression by inhibiting epithelial-to-mesenchymal transition in NQO1-positive breast cancers. *Sci Rep.* 2017;7(1):2681.
34. Zhao W, Jiang L, Fang T, Fang F, Liu Y, Zhao Y, et al. beta-Lapachone selectively kills hepatocellular carcinoma cells by targeting NQO1 to induce extensive DNA damage and PARP1 hyperactivation. *Front Oncol.* 2021;11:747282.
35. Lee HW, Seong SJ, Ohk B, Kang WY, Gwon MR, Kim BK, et al. Pharmacokinetic and safety evaluation of MB12066, an NQO1 substrate. *Drug Des Devel Ther.* 2017;11:2719-25.
36. Zada S, Hwang JS, Ahmed M, Lai TH, Pham TM, Kim DH, et al. Protein kinase A activation by beta-Lapachone is associated with apoptotic cell death in NQO1-overexpressing breast cancer cells. *Oncol Rep.* 2019;42(4):1621-30.

37. Chen Y, Wu R, Li X, Cao M, Yang M, Fu B, et al. beta-Lapachone, an NQO1 bioactivatable drug, prevents lung tumorigenesis in mice. *Eur J Pharmacol.* 2024;973:176511.
38. Zhao L, Miao H, Quan M, Wang S, Zhang Y, Zhou H, et al. beta-Lapachone induces ferroptosis of colorectal cancer cells via NCOA4-mediated ferritinophagy by activating JNK pathway. *Chem Biol Interact.* 2024;389:110866.
39. Du P, Li Y, Han A, Wang M, Liu J, Piao Y, et al. beta-Lapachone suppresses carcinogenesis of cervical cancer via interaction with AKT1. *Front Pharmacol.* 2025;16:1509568.
40. Bey EA, Bentle MS, Reinicke KE, Dong Y, Yang CR, Girard L, et al. An NQO1- and PARP-1-mediated cell death pathway induced in non-small-cell lung cancer cells by beta-lapachone. *Proc Natl Acad Sci U S A.* 2007;104(28):11832-7.
41. Blanco E, Bey EA, Khemtong C, Yang SG, Setti-Guthi J, Chen H, et al. Beta-lapachone micellar nanotherapeutics for non-small cell lung cancer therapy. *Cancer Res.* 2010;70(10):3896-904.
42. Jeon YJ, Bang W, Choi YH, Shim JH, and Chae JI. Beta-Lapachone suppresses non-small cell lung cancer proliferation through the regulation of specificity protein 1. *Biol Pharm Bull.* 2015;38(9):1302-8.
43. Ma X, Huang X, Moore Z, Huang G, Kilgore JA, Wang Y, et al. Esterase-activatable beta-lapachone prodrug micelles for NQO1-targeted lung cancer therapy. *J Control Release.* 2015;200:201-11.

44. Basters A, Geurink PP, Rocker A, Witting KF, Tadayon R, Hess S, et al. Structural basis of the specificity of USP18 toward ISG15. *Nat Struct Mol Biol*. 2017;24(3):270-8.
45. Jové V, Wheeler H, Lee CW, et al. Type I interferon regulation by USP18 is a key vulnerability in cancer. *iScience*, 2024 Mar 27;27(4):109593.
46. Wu Y, Wang X, Chang S, Lu W, Liu M, Pang X.  $\beta$ -Lapachone Induces NAD(P)H:Quinone oxidoreductase-1– and oxidative stress–dependent heat shock protein 90 cleavage and inhibits tumor growth and angiogenesis. *J Pharmacol Exp Ther*. 2016;357:466-475.
47. Basters A, Ketscher L, Deuerling E, Arkona C, Rademann J, Knobloch KP, et al. High yield expression of catalytically active USP18 (UBP43) using a Trigger Factor fusion system. *BMC Biotechnol*. 2012;12:56.
48. Abramson J, Adler J, Dunger J, Evans R, Green T, Pritzel A, et al. Addendum: Accurate structure prediction of biomolecular interactions with AlphaFold 3. *Nature*. 2024;636(8042):E4.
49. Head MS, Given JA, and Gilson MK. "Mining minima": Direct computation of conformational free energy. *J Phys Chem A*. 1997;101(8):1609-18.
50. David L, Luo R, and Gilson MK. Ligand-receptor docking with the Mining Minima optimizer. *J Comput Aided Mol Des*. 2001;15(2):157-71.
51. Kairys V, and Gilson MK. Enhanced docking with the mining minima optimizer: Acceleration and side-chain flexibility. *J Comput Chem*. 2002;23(16):1656-70.
52. Chen W, Gilson MK, Webb SP, and Potter MJ. Modeling protein-ligand binding by mining Minima. *J Chem Theory Comput*. 2010;6(11):3540-57.

53. Gilson MK, Stewart LE, Potter MJ, and Webb SP. Rapid, accurate, ranking of protein-ligand binding affinities with VM2, the second-generation mining minima method. *J Chem Theory Comput.* 2024;20(14):6328-40.
54. Maier JA, Martinez C, Kasavajhala K, Wickstrom L, Hauser KE, and Simmerling C. ff14SB: Improving the accuracy of protein side chain and backbone parameters from ff99SB. *J Chem Theory Comput.* 2015;11(8):3696-713.
55. Wang JM, Wolf RM, Caldwell JW, Kollman PA, and Case DA. Development and testing of a general amber force field. *J Comput Chem.* 2004;25(9):1157-74.
56. Case DA, Cheatham TIII, Darden T, Gohlke H, Luo R, Merz KJr, et al. The Amber biomolecular simulation programs. *J Comput Chem.* 2005;26(16):1668-88.
57. Tian C, Kasavajhala K, Belfon KAA, Raguetta L, Huang H, Migués AN, et al. ff19SB: Amino-acid-specific protein backbone parameters trained against quantum mechanics energy surfaces in solution. *J Chem Theory Comput.* 2020;16(1):528-52.
58. Li Z, Song LF, Li PF, and Merz K. Systematic parametrization of divalent metal ions for the OPC3, OPC, TIP3P-FB, and TIP4P-FB water models. *J Chem Theory Comput.* 2020;16(7):4429-42.
59. Izadi S, Anandakrishnan R, and Onufriev AV. Building water models: a different approach. *J Phys Chem Lett.* 2014;5(21):3863-71.
60. Berendsen HJC, Postma JPM, Vangunsteren WF, Dinola A, and Haak JR. Molecular-dynamics with coupling to an external bath. *J Chem Phys.* 1984;81(8):3684-90.
61. The PyMOL Molecular graphics system, Version 3.0. *Schrodinger, LLC.*

62. Schwartzenburg J, Juncker, M, Reed R, Desai S. Increased ISGylation in cases of TBI-exposed ALS veterans. *J Neuropathol Exp Neurol*, 78:209-218, 2019.
63. Tyutyunyk-Massey L, Chen Z, Liu X, Kawakami M, Harned A, Ng Y, et al. CDK2 inhibition produces a persistent population of polyploid cancer cells. *JCI Insight*. 2025;10(10).
64. Kawakami M, Mustachio LM, Chen Y, et al. A novel CDK2/9 inhibitor CYC065 causes anaphase catastrophe and represses proliferation, tumorigenesis, and metastasis in aneuploid cancers. *Mol Cancer Ther*. 2021; 20(3):477-489

### Figure legend

**Figure 1:** High-throughput screen identifies candidate USP18 small molecule inhibitors.

(A) The features of the 79,493-compound library used for high-throughput screening is displayed, showing the proportions of fragment, kinase, diversity, biologically annotated, and academic compound sets that were interrogated. (B) The diagram of the fluorogenic enzymatic assay used to identify small-molecule USP18 inhibitors is shown. Recombinant, enzymatically active recombinant USP18 deconjugated ISG15-AMC substrate, and fluorescence intensity was used to calculate the percentage inhibition of each tested compound. (C) Schematic representation of the GFP-tagged USP18 expression vector used to generate enzymatically active USP18 protein. (D) Immunoblot analysis of USP18 species before and after 3C protease cleavage confirmed the production of the enzymatically active USP18 used for the biochemical assays. (E) Workflow of the screening strategy indicated the progression from primary screening to hit validation, including the selection of 13 primary hits, 3 reproducible USP18-inhibitory compounds, and identification of  $\beta$ -lapachone as the lead compound

for further evaluation. **(F)** Dose–response inhibition curves of  $\beta$ -lapachone, 9,10-phenanthrenequinone, and 2-nitrophenanthrene-9,10-dione are displayed using the same fluorogenic enzymatic assay described in panel **B**. **(G)** The percent of ROS production was measured in human A549 and H1299 lung cancer cell lines following  $\beta$ -lapachone treatment at the indicated concentrations with or without co-treatment with the ROS scavenger N-acetylcysteine (NAC, 10 mM). Two-tailed Student's t tests compared differences between arms with a P-value < 0.05 deemed statistically significant. Error bars represent standard deviations with the symbols indicating \* P < 0.05 and \*\* P < 0.01, respectively.

**Figure 2:**  $\beta$ -lapachone reduces lung cancer cell proliferation and increases apoptosis. **(A)** Proliferation and **(B)** apoptosis assays of human lung cancer A549 and H1299 lung cancer cell lines following  $\beta$ -lapachone treatment at the indicated concentrations are displayed.  $\beta$ -lapachone treatment statistically-significantly reduced proliferation and augmented apoptosis in a dose-dependent manner as compared to vehicle controls. **(C)** Apoptosis and proliferation were displayed for A549 lung cancer cells following  $\beta$ -lapachone treatment (versus vehicle treatment) at the indicated concentrations with or without co-treatment with the ROS scavenger N-acetylcysteine (NAC, 10 mM).  $\beta$ -lapachone increased apoptosis significantly at the 4 $\mu$ M dosage, but not at lower concentrations. NAC co-treatment statistically significantly antagonized this effect only at the 4 $\mu$ M dosage. **(D)** Growth suppression by  $\beta$ -lapachone treatment was also antagonized by engineered gain of USP18 expression.  $\beta$ -lapachone treatment repressed proliferation of A549 and H1299 lung cancer cells transfected with an empty

vector (EV). In contrast, USP18 over-expression partially reversed this growth inhibition at the 2 $\mu$ M and 4 $\mu$ M dosages. (E) *In vivo* anti-tumor activity of  $\beta$ -lapachone treatment is displayed at the left panel (12.5 mg/kg or 25 mg/kg body weight) as evaluated using the H1299 human lung cancer xenograft model. The 25 mg/kg body weight of  $\beta$ -lapachone statistically-significantly reduced tumor growth as compared to vehicle-treated controls after 29 days of treatment. Survival is shown in the right panel (F) Representative Hematoxylin and Eosin (H & E) staining, Ki-67 immunostaining, and apoptosis scoring are displayed for different treatment groups. Two-tailed Student's t tests compared differences between study groups with a P-value below 0.05 deemed statistically significant. Error bars represent standard deviations with the symbols indicating \* P < 0.05, \*\* P < 0.01, and \*\*\* P < 0.001, respectively.

**Figure 3:**  $\beta$ -lapachone antagonizes USP18-dependent activity. (A) Interferon-stimulated response element (ISRE) reporter assays were performed to evaluate the effect of  $\beta$ -lapachone treatment on interferon pathway activation. A549 lung cancer cells were transiently transfected with an insertless vector (EV) as a control or a USP18 expression vector and treated with the indicated concentrations of  $\beta$ -lapachone with or without interferon (200 Units) co-treatment.  $\beta$ -lapachone treatment statistically-significantly increased ISRE reporter activity in a concentration-dependent manner, whereas USP18 overexpression antagonized this activation. (B) Immunoblot analyses were performed to assess the effects of  $\beta$ -lapachone treatment on global ISGylation in A549 cells. Representative immunoblot images and the quantification of conjugated ISG15 species within the indicated bracketed region of four independent experiments

are displayed. A statistically significant increase in global ISGylation was evident after dose-dependent  $\beta$ -lapachone treatments. (C) Independent immunoblot analyses of NEDD8, ubiquitin, and SUMO-2/3 conjugation after  $\beta$ -lapachone treatment as compared to vehicle control were performed to evaluate pathway selectivity.  $\beta$ -lapachone treatment did not confer detectable changes in ubiquitin or NEDD8 conjugation. Only a modest change in SUMO-2/3 conjugation was observed at the highest  $\beta$ -lapachone concentration. The vinculin signals present in the middle and right panels were from the same immunoblot and lysate that were independently probed for ubiquitin and SUMO-2/3. The NEDD8 immunoblot was from a different lysate. These immunoblots present representative signals for each of these species. (D) Quantification of the NEDD8, ubiquitin, and SUMO-2/3 conjugates shown in (C) was performed using three independent replicate experiments. Two-tailed Student's t tests compared differences between study groups with a P-value below 0.05 deemed statistically significant. Error bars represent standard deviations with the symbols indicating \* P < 0.05, \*\* P < 0.01, \*\*\* P < 0.001 and \*\*\*\* P < 0.0001, respectively.

**Figure 4:** Molecular modeling of  $\beta$ -lapachone binding to USP18. (A) Structural modeling of USP18 and ISG15 complex formation identified a hydrophobic pocket in USP18 required for substrate engagement. Within this pocket, three key amino acid residues—D139, F259, and T266 were found to mediate ISG15 binding. (B) Molecular docking analysis revealed that  $\beta$ -lapachone (green) interacts with USP18 at the identified hydrophobic pocket, with the critical residues D139, F259, and T266 highlighted in brown. (C) Docking simulations of  $\beta$ -lapachone, 9,10-phenanthrenequinone, and 2-

nitrophenanthrene-9,10-dione showed that all three compounds occupy this same hydrophobic pocket of USP18 in a similar spatial configuration. **(D)** Calculated binding energies for  $\beta$ -lapachone, 9,10-phenanthrenequinone, and 2-nitrophenanthrene-9,10-dione are individually displayed, supporting comparable affinities for binding to USP18 protein.

**Figure 5:** Mutational analyses validate the USP18 residues critical for  $\beta$ -lapachone binding and activity. **(A)** Binding energy calculations and 1,000 nanosecond molecular dynamics simulations were performed to evaluate the effects of single (D139K, F259K, T266K), double, and triple amino acid substitutions on  $\beta$ -lapachone–USP18 interactions. Mutation of any of the three key residues markedly reduced predicted binding affinity, with the triple mutant (D139K/F259K/T266K) abolishing stable binding. **(B)** Molecular dynamics visualization of  $\beta$ -lapachone (green) bound to wild-type and mutant USP18 proteins (blue) after 1,000 nanosecond simulations showed stable binding to wild-type USP18 but with ejection of  $\beta$ -lapachone from mutant USP18 species. **(C)** Immunoblot analysis confirmed comparable expression of wild-type and mutant USP18 proteins following transfection of each construct, including single and triple mutants. **(D)** The A549 lung cancer cell line was transfected with an ISRE luciferase reporter plasmid together with either empty vector, wild-type USP18, or USP18 constructs harboring individual (D139K, F259K, T266K) or triple mutations at the indicated residues. Luciferase activity was measured 48 hours post-transfection and normalized to Renilla luciferase. Two-tailed Student's t tests compared differences between study groups with a P-value below 0.05 deemed statistically significant. Error

bars represent standard deviations with the symbols indicating \*  $P < 0.05$  and \*\*  $P < 0.01$ , respectively.

**Figure 6:** Transcriptomic profiling identifies USP18-dependent gene expression changes conferred by  $\beta$ -lapachone treatment relative to vehicle control. **(A)** Volcano plot displayed the differentially expressed genes in A549 human lung cancer cells treated with  $\beta$ -lapachone (2.5 $\mu$ M) as compared to vehicle-treated controls.  $\beta$ -lapachone treatment caused distinct patterns of gene up-regulation and down-regulation. **(B)** Volcano plot of A549 lung cancer cells engineered to over-express USP18 versus empty vector controls is shown following  $\beta$ -lapachone treatment (2.5 $\mu$ M) as compared to vehicle control. Genes whose expression changes were opposed by USP18 over-expression represent  $\beta$ -lapachone regulated transcripts that are USP18-dependent. **(C)** Quantitative real-time PCR assays validated representative  $\beta$ -lapachone regulated genes identified in panel **B**, including those decreased (NR4A2, ENTPD1, DCC, and USP41) and those increased (FGF13, IL31RA, OTUD7A, and KLK2) after  $\beta$ -lapachone treatment. **(D)** Representative  $\beta$ -lapachone treatment repressed expression of USP18-dependent genes, including LINC00319, NCCRP1, and ENTPD1. Differential expression profiles of many of species showed statistically-significant associations with overall survival in TCGA lung adenocarcinoma cohort. **(E)** Representative  $\beta$ -lapachone treatment increased expression of USP18-regulated genes, including FGF13, IL31RA, OTUD7A, and KLK2, exhibited statistically-significant associations with improved overall survival in the same TCGA cohort. Two-tailed Student's t tests compared differences between study groups with a P-value below 0.05 deemed statistically significant. Error

bars represent standard deviations with the symbols indicating \*  $P < 0.05$ , \*\*  $P < 0.01$  and \*\*\*  $P < 0.001$ , respectively. Survival analyses for panels **D** and **E** were performed using the Kaplan–Meier method using the log-rank test with a P-value below 0.05 deemed statistically significant.

**Figure 7:** Proteomic analyses reveal  $\beta$ -lapachone treatment affected ISG15-related proteins. **(A)** ISG15 immunoprecipitation followed by mass spectrometry proteomics analysis was performed in A549 lung cancer cells that expressed an empty vector or a USP18 expression construct and these transfectants were treated with  $\beta$ -lapachone (2.5 $\mu$ M) or vehicle treatments. Comparative proteomic analyses identified potential ISG15-conjugated proteins whose levels were increased by  $\beta$ -lapachone and rescued by engineered USP18 over-expression. Among the ISG15-conjugated targets detected, 86 were previously reported ISG15 substrates, and 70 were found as new ISG15-conjugated proteins. **(B)** Functional categorization of the  $\beta$ -lapachone treatment arm that regulated ISG15 conjugates revealed broad distribution across multiple cellular processes. **(C)** Immunoblot validation of the representative ISG15-conjugated protein, DYNLL1, confirmed that its expression was regulated by  $\beta$ -lapachone-treatment relative to vehicle controls (quantification is shown). Error bars represent standard deviations with the symbols indicating \*  $P < 0.05$ , \*\*  $P < 0.01$ , and \*\*\*  $P < 0.001$ , respectively. **(D)** TCGA lung adenocarcinoma cohort analyses demonstrated that several  $\beta$ -lapachone upregulated ISG15-conjugated proteins, including DYNLL1, HAUS6, LAMB3, BANF1, EIF5A, and ANXA2P2, were statistically-significantly associated with lung cancer survival outcomes. **(E)** Four previously unrecognized ISG15-conjugated proteins,

PCBP2, NME1, TUBA1C, and TUBA4A, were confirmed as  $\beta$ -lapachone regulated ISG15 targets whose elevated expression predicted an unfavorable survival in TCGA lung adenocarcinoma cases. Survival analysis for panels **D** and **E** highlighted species was performed using the Kaplan–Meier method using the log-rank test with a P-value below 0.05 deemed statistically significant.

# Figure 1

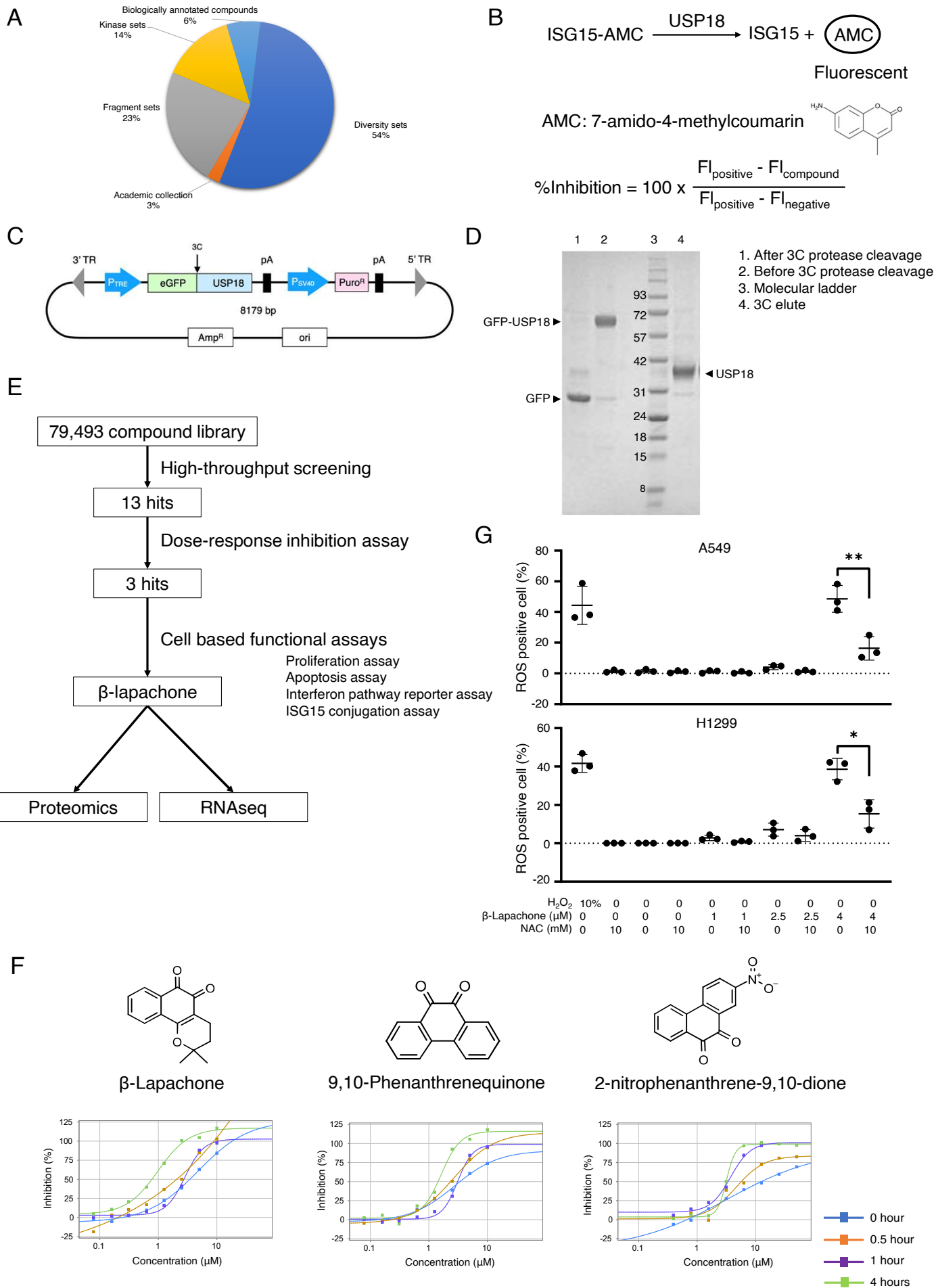


**Figure 2**

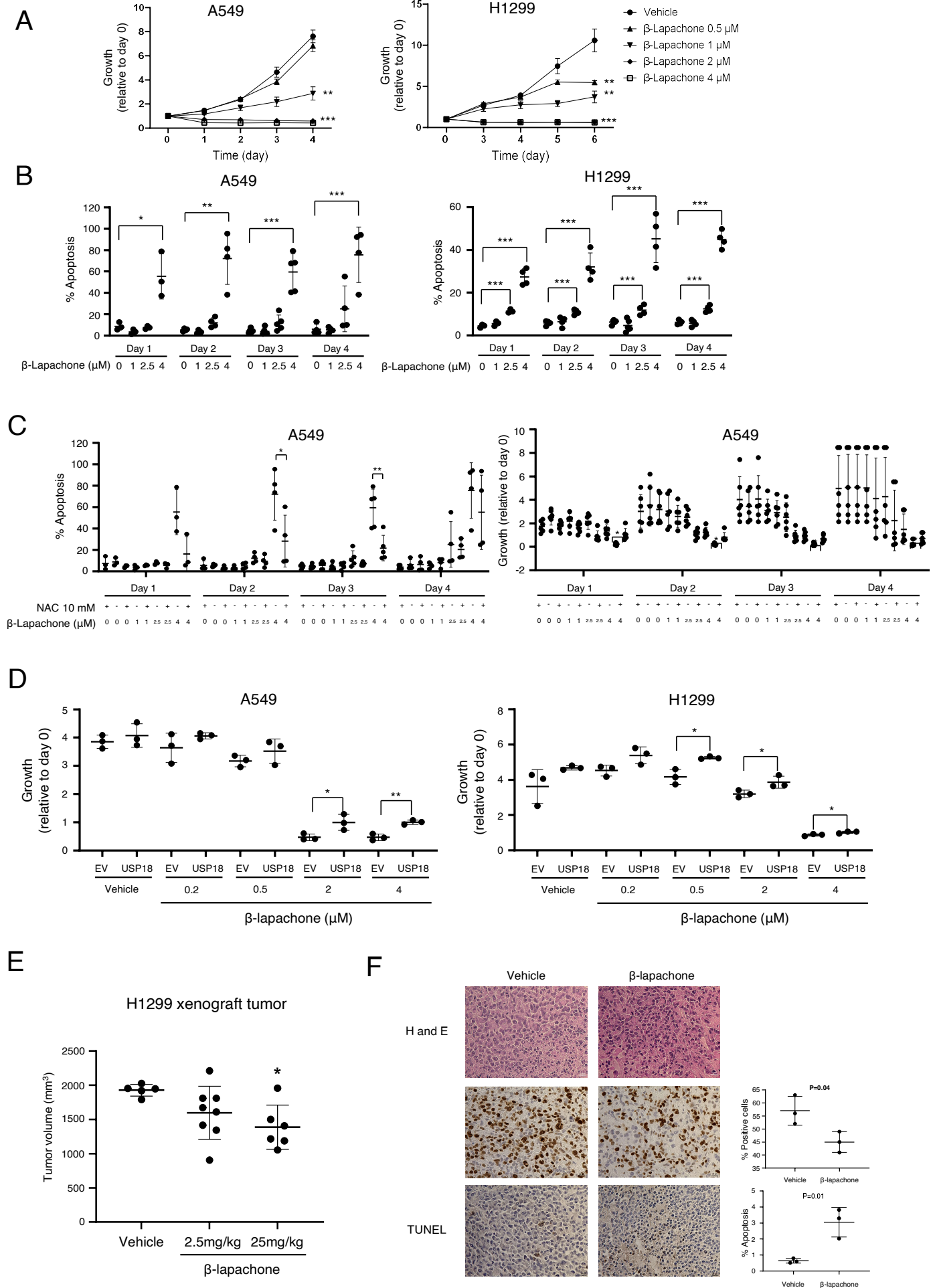
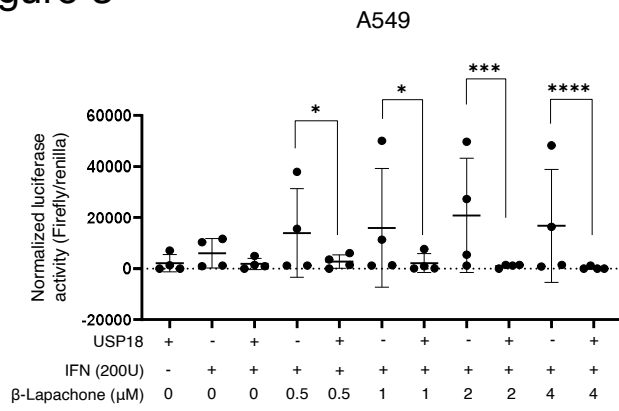
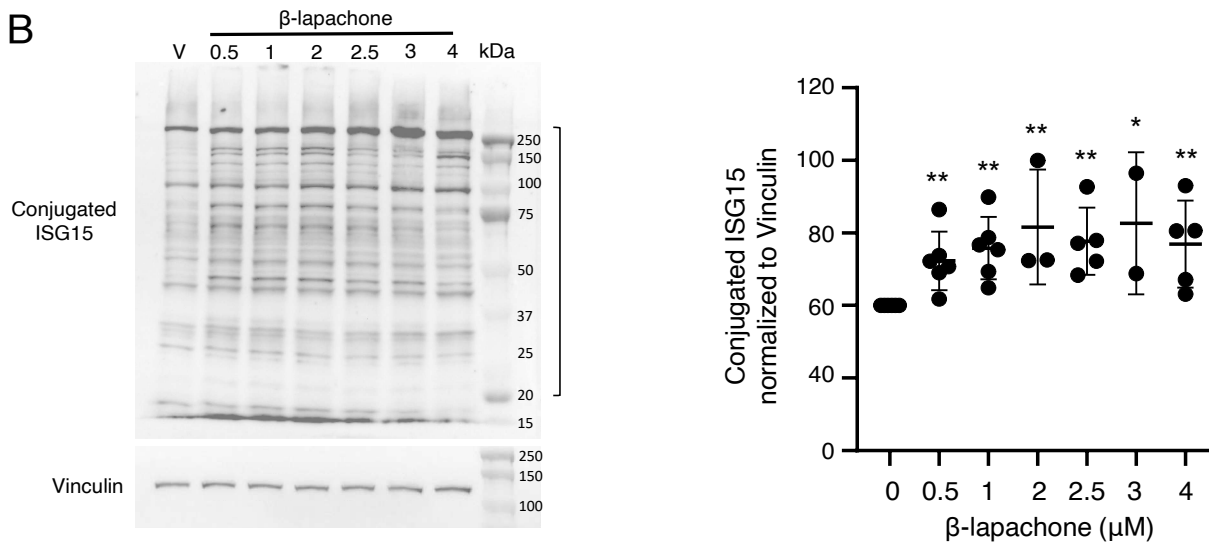


Figure 3

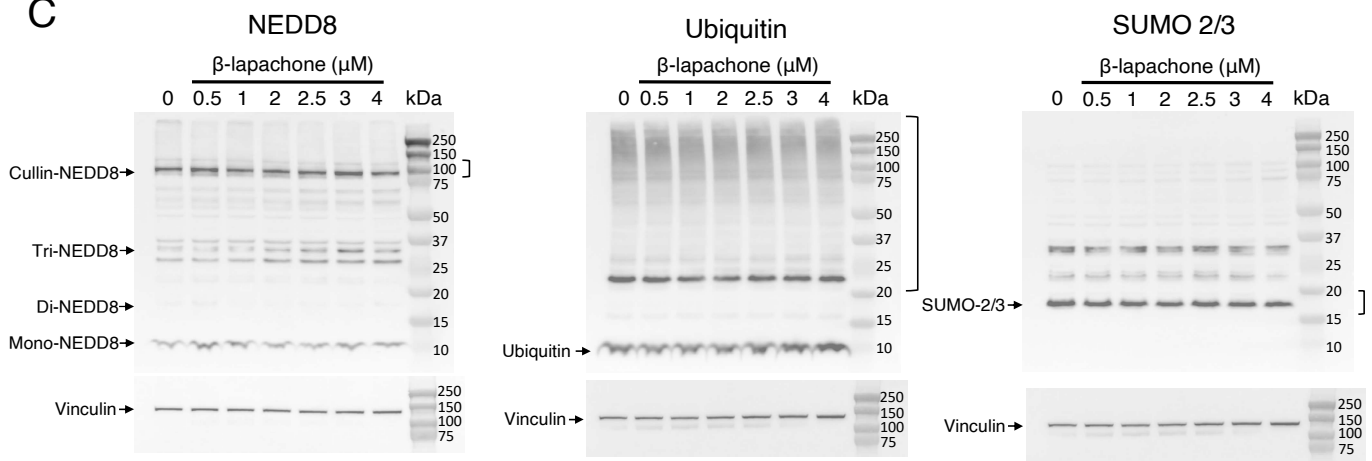
A



B



C



D

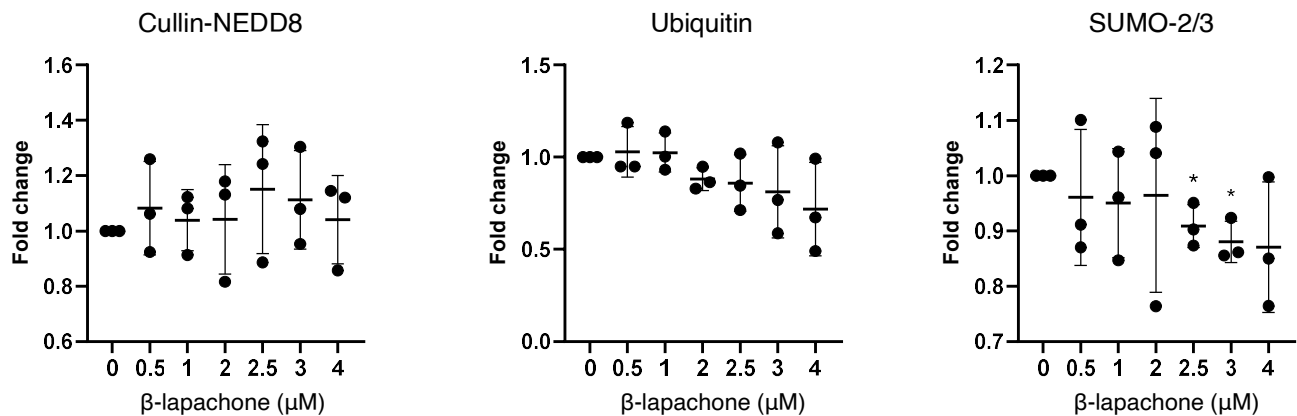
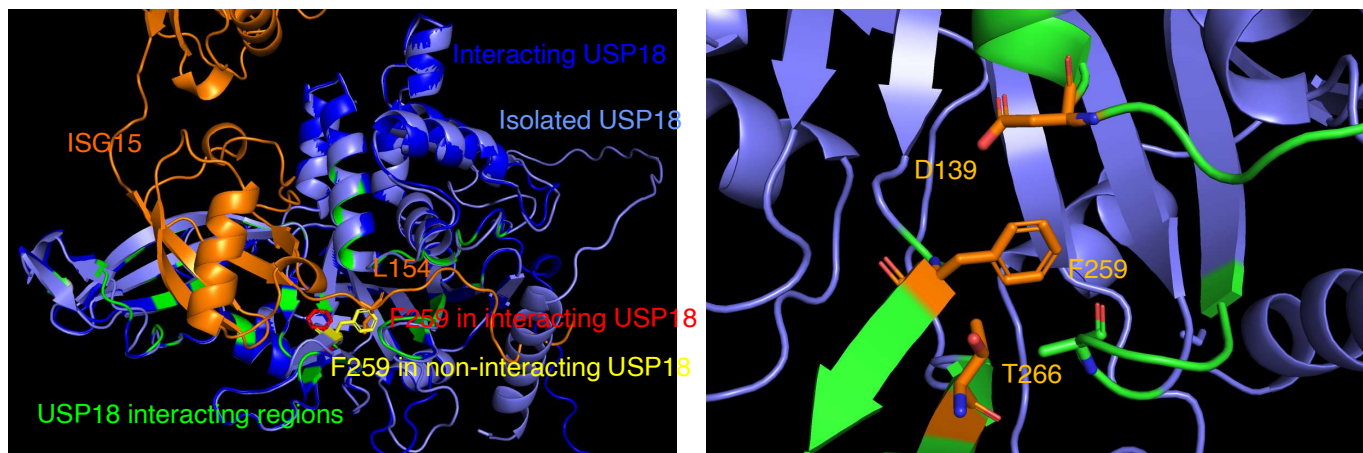
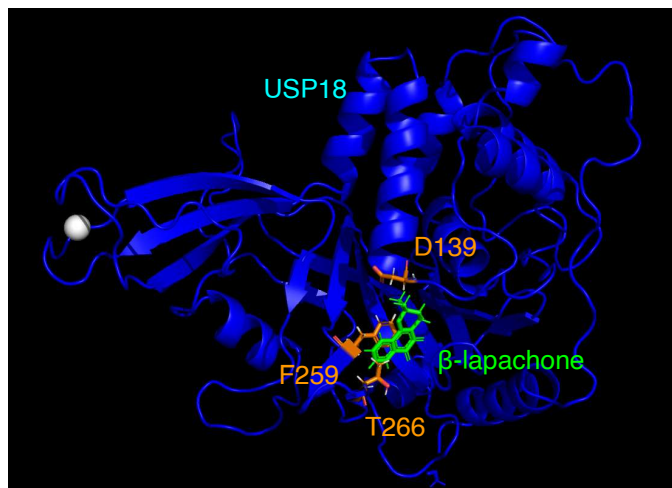


Figure 4

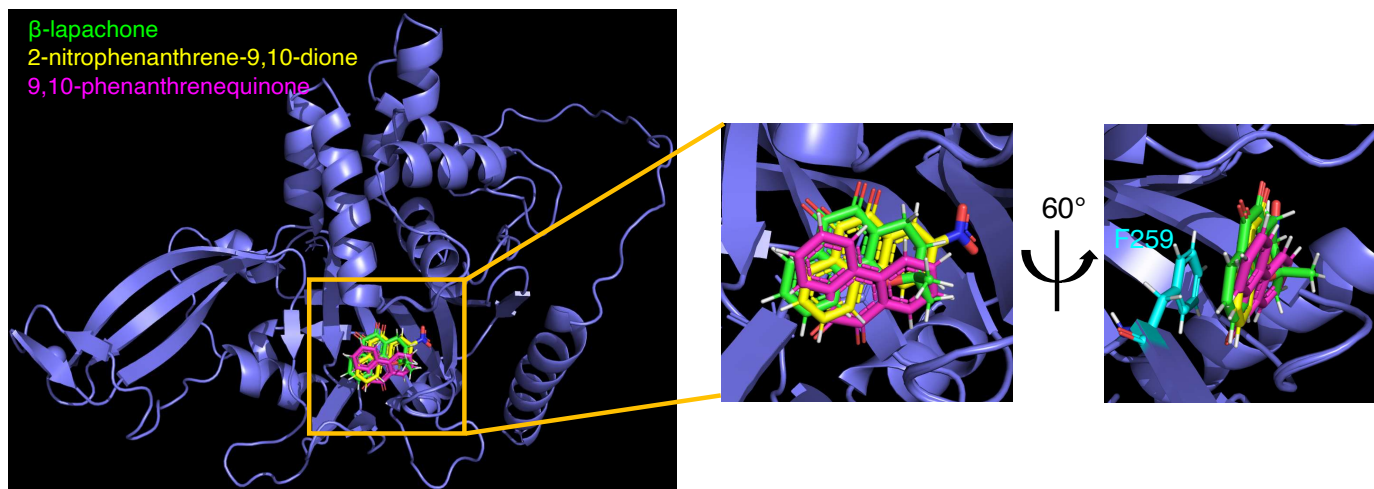
A



B



C



D

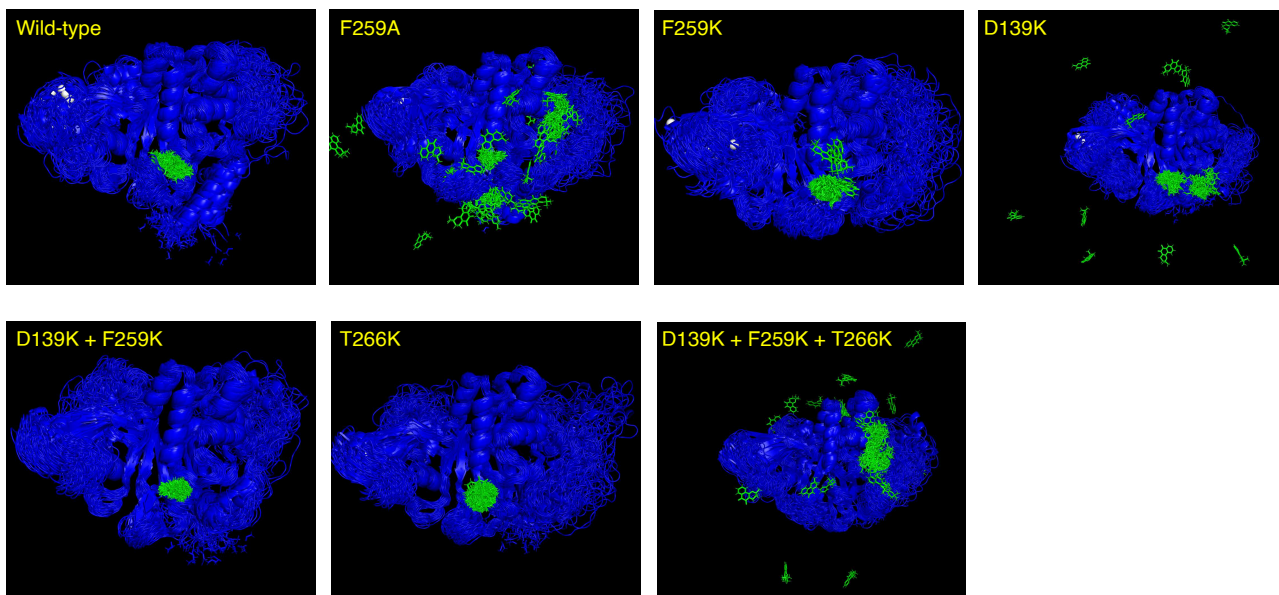
Ligands	Binding energy (kcal/mol)
$\beta$ -lapachone	-6.1
2-nitrophenanthrene-9,10-dione	-7.8
9,10-phenanthrenequinone	-7.4

Figure 5

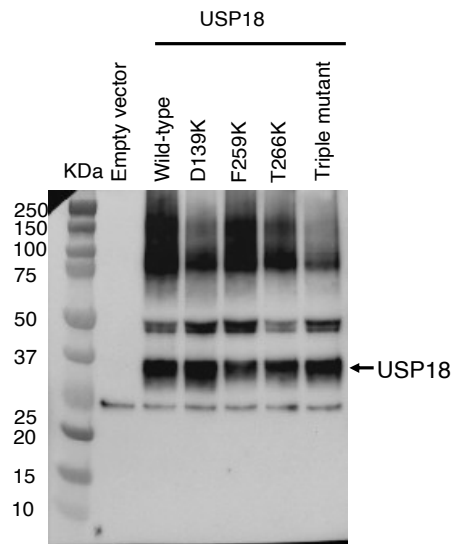
A

Amino acids	$\beta$ -Lapachone binding energy (kcal/mol)	Simulation results
Wild-type F259 and D139	-5.9	stable
F259A and Wild-type D139	-3.6	ejection
F259K and Wild-type D139	-2.4	stable
Wild-type F259 and D139K	-0.7	ejection
F259K and D139K	+7.6	stable
Wild-type T266	-5.9	stable
T266K	-3.0	stable
D139K, F259K and T266K	+14.7	ejection

B



C



D

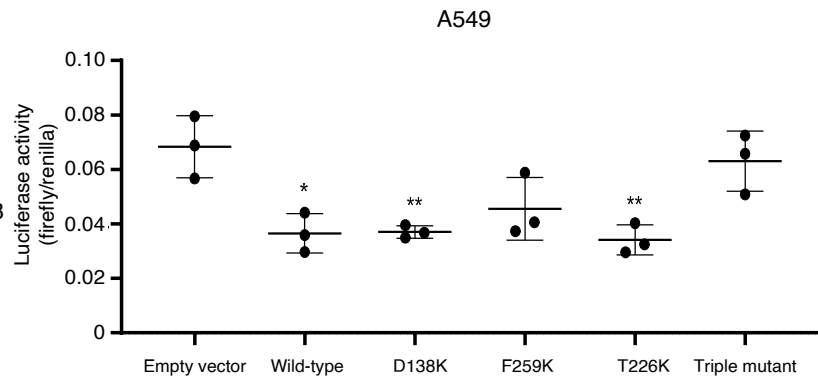


Figure 6

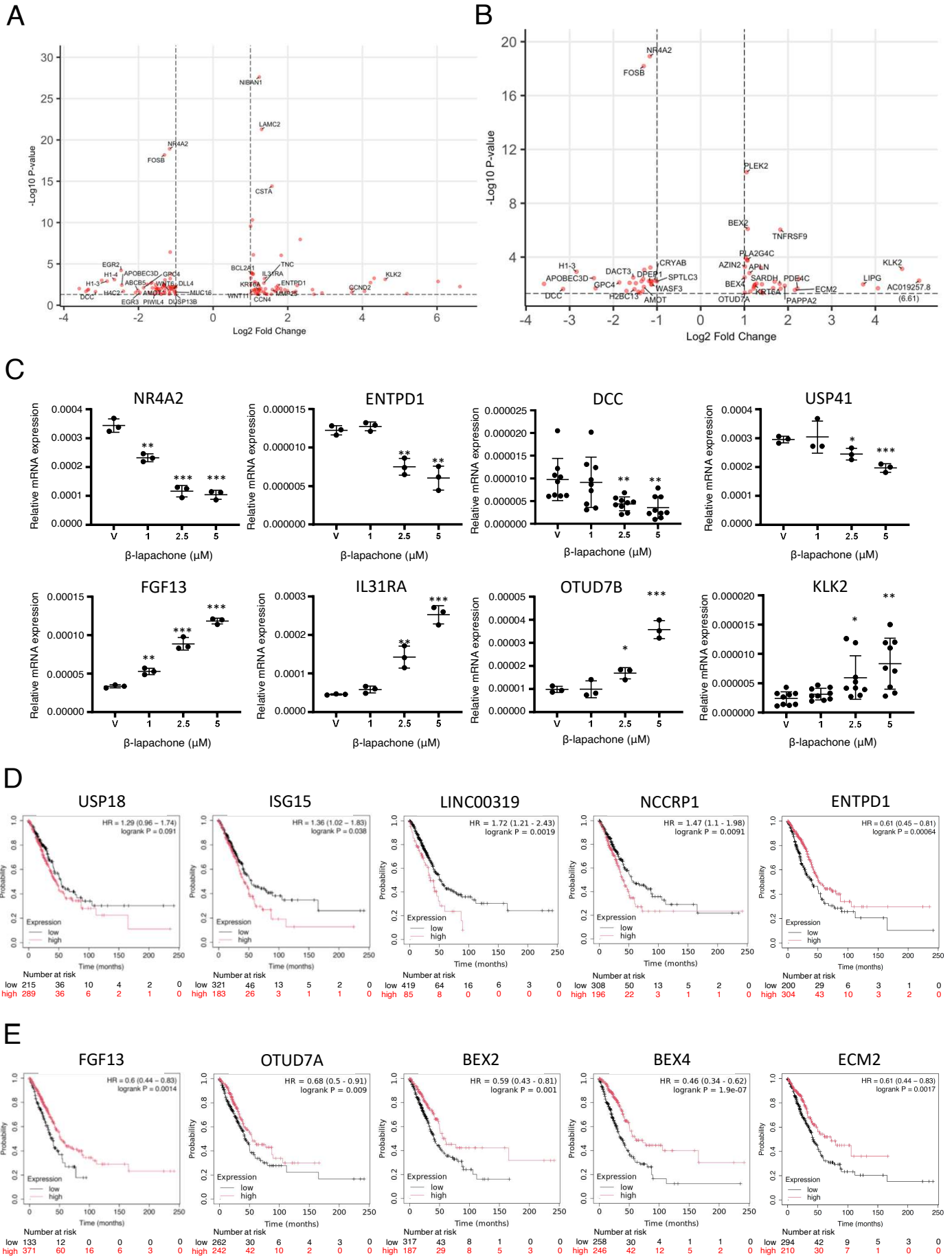


Figure 7

